**Title**
A comprehensive phenotypic CRISPR-Cas9 screen of the ubiquitin pathway uncovers roles of ubiquitin ligases in mitosis



**Author**
Hundley, Frances

**Publication Date**
2020

A comprehensive phenotypic CRISPR-Cas9 screen of the ubiquitin pathway uncovers roles of ubiquitin ligases in mitosis

by
Frances Hundley

DISSERTATION
Submitted in partial satisfaction of the requirements for degree of
DOCTOR OF PHILOSOPHY

in

Biochemistry and Molecular Biology

in the

GRADUATE DIVISION
of the
UNIVERSITY OF CALIFORNIA, SAN FRANCISCO

Approved:

DocuSigned by:
David Toczyski
B39DA64A208E4CB...

David Toczyski
Chair

DocuSigned by:
Natalia Jura
[illegible]2F...

Natalia Jura

DocuSigned by:
David Morgan
AAC13F29657E472...

David Morgan

Committee Members

## Acknowledgements

I would like to thank my mentors, colleagues, friends, and family for their guidance and tireless support throughout my time in graduate school. Without your help, this would not have been possible.

As a high school student, I had the amazing opportunity to work in a biology lab at Los Alamos National Laboratory under the mentorship of Dr. Momchilo Vuyisich. Momo taught me the fundamentals of experimentation, but more importantly, he taught me how exciting working in a lab can be and helped me find a career path I love. At Pomona College, my scientific mentors Dr. Len Seligman, Dr. Matthew Sazinsky, Dr. Tina Negritto, and others, helped me home in on the specific areas of biology I was most interested in pursuing and provided helpful advice about applying to graduate school.

All of the current and former Toczyski lab members made the lab a great place to work, where we could discuss everything from the latest innovative paper to the current political crisis to the proper definitions of peruse and fungible. I learned a great deal from all of my T lab colleagues, and I think I am a better scientist now because of them. In particular, my rotation mentor Theresa Berens Loveless taught me all about ubiquitin ligases, working with tissue culture cells, and how to be a careful, thoughtful scientist. Emma Alme, Jessica Lao, Kevin Mark, Fernando Meza Gutierrez, and Katie Ulrich gave helpful suggestions for relevant background information in the literature, troubleshooting experiments, and navigating the non-scientific parts of working in science. This project was a team effort, and I am grateful to have been part of such an intelligent, hardworking, and fun team of scientists: thank you Nerea Sanvisens Delgado, Harold Marin, and Kaili Carr. I have made what I hope will be lifelong friendships from my time in the T lab.

I would like to thank my thesis advisor Dr. Dave Toczyski for being a fantastic mentor, inspiring scientist, and interesting conversationalist. Although I cannot always keep up with his impressive mental math and back-of-the-envelope calculations, I have gotten better over the years and will continue working towards matching his skill level in this area. He has taught me how to design a good experiment (big or small), to challenge my assumptions, and to get over my fear of asking questions in front of an audience. Graduate school, in large part because of Dave's mentorship and encouragement, has enabled me to

regain my self-confidence, and I cannot overstate how transformative this has been in my life, both in and outside the lab. Getting a PhD in an experimental science is a long process, and one that often feels impossible because the end goal is far away and so much troubleshooting is required before something of significance is finally achieved. Dave's constant optimism in the face of experimental challenges was often just what I needed to keep pushing through to the end. I will miss working with Dave, and I am grateful I had the opportunity to be one of his graduate students.

I would like to thank my thesis committee members Dr. Natalia Jura and Dr. David Morgan for their scientific and career advice and for providing helpful, alternative perspectives on project direction.

My Tetrad classmates, many of whom are now good friends, helped me get through the challenging first year of graduate school and beyond. My non-scientist friends from Pomona College and New Mexico were consistently encouraging and provided much needed perspective.

I would like to thank my family, who have always supported me and my goals, even when graduate school seemed endless and the esoteric details of scientific publishing were confusing. My mom was always willing to listen when I was frustrated about the progress of my experiments. My dad—a physicist—exposed me to science when I was growing up with fun projects like building a DC electric motor together and trips to his lab where he would pour liquid nitrogen on the floor so I could watch the droplets race across the room, picking up dust along the way. He and my bonus-mom are always there for me with thoughtful advice, and Pam has been an advocate for me throughout my education. During my time in graduate school, my brother Val has become a biologist as well, and it has been great to talk about our research, along with other random, fascinating topics. Finally, I would like to thank my grandparents, Richard and Janna Hundley, who passed away before I graduated from college and started graduate school, but who always believed in my ability to earn a PhD. My grandfather's life and academic achievements were inspiring to me, and he was one of the smartest people I have ever met. He always advised me to find a career "that you are good at, that you enjoy, and that society values". I am incredibly lucky to be able to say that with the help and support of so many people along the way I think I have found that career.

## Contributions

The work described in Chapter 1 has been submitted for publication in a peer reviewed journal. Frances Hundley led the project in collaboration with David Toczyski, and Frances designed the study, planned experiments, carried out experiments, and analyzed the data in collaboration with Nerea Sanvisens Delgado, Harold Marin, and Kaili Carr. Ruilin Tian conducted the FDR analysis. Frances Hundley wrote the manuscript in collaboration with David Toczyski. David Toczyski oversaw the project.

## Abstract

**A comprehensive phenotypic CRISPR-Cas9 screen of the ubiquitin pathway uncovers roles of ubiquitin ligases in mitosis**

By Frances V. Hundley

The complex human ubiquitin proteasome system, comprised of over 700 ubiquitin ligases (E3s) and deubiquitinases (DUBs), has been difficult to systematically and phenotypically characterize. We performed a chemical-genetic CRISPR-Cas9 screen to identify E3s/DUBs whose loss renders cells sensitive or resistant to 41 compounds targeting a broad range of biology, including cytoskeletal integrity, mitosis, G1/S progression, genome stability, translation, metabolism, and vesicular transport. Genes and compounds both clustered functionally, showing that inhibitors of related pathways interact similarly with the E3s/DUBs and demonstrating the robustness of our screen. Some genes, such as *FBXW7*, showed interactions with more than one-third of the compounds. Others, such as the mostly un-studied *RNF25* and *FBXO42*, showed interactions primarily with a single compound (MMS for *RNF25*) or a set of related compounds (mitotic cluster for *FBXO42*). Mutation of several E3s with sensitivity to mitotic inhibitors had an increase in aberrant mitoses, suggesting a role for these genes in cell cycle regulation. Overall, our comprehensive CRISPR-Cas9 screen uncovered 466 gene-compound interactions covering 25% of the E3s/DUBs interrogated.

## Table of Contents

## List of Figures

### Chapter 1

## List of Tables

### Chapter 1

## List of Supplementary Files

### Chapter 1

# Chapter 1

## A comprehensive phenotypic CRISPR-Cas9 screen of the ubiquitin pathway uncovers roles of ubiquitin ligases in mitosis

**A comprehensive phenotypic CRISPR-Cas9 screen of the ubiquitin pathway uncovers roles of ubiquitin ligases in mitosis**

Frances V. Hundley[1,2], Nerea Sanvisens Delgado[1], Harold C. Marin[1,2], Kaili L. Carr[1], Ruilin Tian[1], and David P. Toczyski[1]

1. University of California, San Francisco, San Francisco, CA 94158, USA

2. Tetrad Graduate Program, University of California, San Francisco, San Francisco, CA 94158, USA

**Abstract**

The complex human ubiquitin proteasome system, comprised of over 700 ubiquitin ligases (E3s) and deubiquitinases (DUBs), has been difficult to systematically and phenotypically characterize. We performed a chemical-genetic CRISPR-Cas9 screen to identify E3s/DUBs whose loss renders cells sensitive or resistant to 41 compounds targeting a broad range of biology, including cytoskeletal integrity, mitosis, G1/S progression, genome stability, translation, metabolism, and vesicular transport. Genes and compounds both clustered functionally, showing that inhibitors of related pathways interact similarly with the E3s/DUBs and demonstrating the robustness of our screen. Some genes, such as *FBXW7*, showed interactions with more than one-third of the compounds. Others, such as the mostly un-studied *RNF25* and *FBXO42*, showed interactions primarily with a single compound (MMS for *RNF25*) or a set of related compounds (mitotic cluster for *FBXO42*). Mutation of several E3s with sensitivity to mitotic inhibitors had an increase in aberrant mitoses, suggesting a role for these genes in cell cycle regulation. Overall, our comprehensive CRISPR-Cas9 screen uncovered 466 gene-compound interactions covering 25% of the E3s/DUBs interrogated.

## INTRODUCTION

To respond rapidly to changing internal and external conditions, cells transform their proteome through post-translational modifications (PTMs), which allows alteration of the existing pool of proteins. Numerous PTMs have been characterized, from phosphorylation and acetylation to ubiquitination, arguably the most versatile of all PTMs. Ubiquitin is an evolutionarily conserved 8.5kDa protein that is covalently attached to the N-terminal or lysine residues of substrate proteins through a sequential reaction involving a ubiquitin activating enzyme (E1), ubiquitin conjugating enzyme (E2), and a ubiquitin ligase (E3) (Ciechanover et al., 1980; Goldstein et al., 1975). Polyubiquitin chains can be built by linking ubiquitin to lysine 48 of ubiquitin itself, leading to substrate degradation by the proteasome (Chau et al., 1989; Thrower et al., 2000). Other types of polyubiquitin chain linkages, as well as mono-ubiquitination, can lead to degradation or can have non-degradative effects on substrates, such as re-localization, promoting protein-protein interactions, and regulating signaling events (Arnason and Ellison, 1994; Meza Gutierrez et al., 2018; Spence et al., 1995).

Ubiquitination is regulated by over 1,000 proteins in humans, representing roughly 4% of the proteome, including two E1s, approximately 40 E2s, over 600 E3s, and approximately 100 deubiquitinases (DUBs) (Clague et al., 2015; Komander et al., 2009; Li et al., 2008). Over 8,000 unique ubiquitination sites on thousands of proteins have been reported, but the true number is likely to be much higher due to difficulties observing this often transient PTM (Rose et al., 2016; Xu and Jaffrey, 2013). E3s are a crucial regulatory node for the process as they typically confer substrate specify to the ubiquitination reaction. There are three main types of E3s, distinguished by catalytic mechanism: HECT, RBR, and RING. The first two participate directly in catalysis

via intermediate conjugation of ubiquitin, whereas RING ligases perform a scaffolding role by bringing ubiquitin-charged E2s into proximity of the substrate (Deshaies and Joazeiro, 2009; Dove and Klevit, 2017; Huibregtse et al., 1995; Scheffner et al., 1995). Several E3s, such as the APC/C, the SCF, and other cullin-RING ligases (CRLs), have established essential roles in cell cycle progression and the DNA damage response (Thornton and Toczyski, 2006). However, the majority of the over 600 ubiquitin E3s in humans have not been well-characterized.

Early comprehensive screens in *S. cerevisiae* used temperature-sensitive alleles to place essential genes into broad biological pathways, such as protein, RNA, and DNA synthesis (Hartwell, 1967), and later work employing systematic *S. cerevisiae* gene deletion collections enabled identification of genetic interactions through generation and analysis of double deletions (Tong et al., 2001). The recent development of CRISPR-Cas9 for genetic screening has enabled high-throughput determination of gene essentiality, cancer cell dependencies, and genetic interactions in human cells (Han et al., 2017; Hart et al., 2015; Horlbeck et al., 2018; Jinek et al., 2012; Wang et al., 2015, 2017). Here, we broadly characterized human E3/DUB functions by performing a pooled CRISPR-Cas9 screen combined with chemical inhibition of numerous pathways using 41 different compounds. In total, we tested the effect of mutation of 629 E3s and 56 DUBs on cell growth in the presence of compounds targeting genome integrity, cell cycle progression, transcription, RNA processing, translation, mitochondrial function, protein folding, proteostasis, metabolic pathways, intracellular transport, cytoskeleton, various signaling pathways, and endoplasmic reticulum function. By probing a diverse set of biological processes for E3 and DUB involvement, we were able to assess the specificity of these interactions. Mutation of 66 E3s/DUBs caused significant enrichment or de-enrichment when grown in the presence of only

one compound, and many others were responsive primarily to a set of compounds targeting one pathway, such as mitosis. Overall, we identified one or more specific interactions for 152 E3s and nine DUBs. We validated over twenty of these observed E3/DUB sensitivities and resistances with independent competitive growth assays. The screen revealed previously unrecognized sensitivity of a putative $CUL5^{WSB2}$ complex to an inhibitor of nuclear export; sensitivity of *FBXO8* to an inhibitor of vesicular transport; specific sensitivity of *RNF25* to methylation-induced damage; and sensitivity of the mostly uncharacterized F-box *FBXO42* and the HECTs *HUWE1* and *UBE3D* to inhibitors of mitosis, to name a few. Further analysis focused on FBXO42, which showed highly specific sensitivity to mitotic inhibitors and defects in mitosis in two distinct cell types. Collectively, our dataset of 28,577 gene-compound interactions represents a critical resource for the study of the ubiquitin pathway and the diverse processes regulated by ubiquitination.

## RESULTS

### CRISPR-Cas9 screen to identify roles of E3s and DUBs across fundamental pathways

To systematically characterize the human ubiquitin proteasome system (UPS), we performed a pooled CRISPR-Cas9 screen across 41 compounds targeting numerous biological processes (Figure 1.1A and 1.1B and Supplementary File 1.S3). We generated a partially-custom UPS sgRNA library of 6,306 sgRNAs, with nine targeting each ubiquitin-related gene, 81 non-targeting control sgRNAs, and 60 targeting control sgRNAs against 20 genes that are not expressed in most cells (Supplementary File 1.S1). The library targets 629 human E3 catalytic components, substrate binding modules, and structural components, as well as 56 non-essential DUBs. To ensure effective cutting, we selected seven previously published sgRNAs (Wang et al., 2015) per gene, in addition to two newly-designed sgRNAs (termed domain-specific sgRNAs) precisely targeting key catalytic or binding residues of each E3 or DUB. Such sgRNAs would be more likely to yield a non-functional protein even if the Cas9-induced double strand break was repaired with an in-frame insertion or deletion (Shi et al., 2015), and may allow us to uncover E3s, such as BRCA1, that have roles independent of their catalytic domains (Reid et al., 2008). We generated four independent doxycycline-inducible Cas9 HAP1 clones and confirmed effective Cas9 induction in each that was resistant to silencing over many weeks in culture (Figure 1.S1). HAP1 cells were chosen for their ease of infection, relatively rapid growth, and established use in CRISPR-Cas9 screening.

Before performing the screen with all 41 compounds, we optimized the screening conditions and timeline with the CDK4/6 inhibitor palbociclib, which inhibits the transition from G1 to S-phase (Fry et al., 2004; Matsushime et al., 1992; Meyerson and Harlow, 1994). By observing cell

confluency in the presence of a range of palbociclib doses, we found that 1.5μM inhibited HAP1 growth to approximately 70% that of untreated cells (Figure 1.1C), a level that allowed us to reveal both rescue and synthetic sensitivity. Next, we performed a trial screen. Briefly, two of the HAP1-Cas9 clones were infected with the sgRNA library in parallel at an MOI of approximately 0.4. Puromycin was used to select for sgRNA integration for four days, and one day after selection was complete, doxycycline was added for three days to induce Cas9. Initial samples were collected after selection, but prior to Cas9 induction (termed "pre-dox" samples). Cells were then split into media with or without palbociclib, and split into fresh inhibitor or control media every two days. Samples were collected at days 0, 2, 4, 8, and 12, and relative sgRNA abundance was determined by Illumina sequencing (Figure 1.1A). Reads were first normalized to pre-dox samples, then Log2(treated/untreated) was calculated for each gene.

Eight days of growth in palbociclib was sufficient to reveal strongly sensitive and resistant E3/DUB mutants that did not differ profoundly from the day 4 or day 12 samples, and the replicates were well-correlated (Figures 1.1D and 1.1E). HAP1 cells double roughly every 16 hours, so eight days is approximately 12 doublings (Figure 1.1C), providing time for growth differences to amplify. Mutations that conferred resistance fell into two categories. Inactivation of some genes, such as *FBXW7* and *RFWD2*, allowed cells to grow better than their wild type counterparts in palbociclib, representing true resistance (Figure 1.1F). In contrast, inactivation of other genes, such as *UBR4*, caused slow growth compared to wild type cells in the control untreated experiment, and the cytostatic compound palbociclib appeared to rescue this sickness (Figure 1.1F). Such mutants are not truly resistant to the compound, as much as rescued by it.

**Mapping E3 and DUB involvement across diverse biological processes**

We next performed the eight day CRISPR-Cas9 screen across all 41 compounds, this time with three independently generated HAP1-Cas9 clones. As with palbociclib, we identified a dose of each compound that reduced apparent growth to approximately 60-70% that of untreated cells (Supplementary File 1.S3). Unbiased, hierarchical clustering of the screen results revealed tightly linked E3/DUB clusters that responded similarly to the panel of compounds (Figure 1.2A, top). These clusters likely result from different relationships. In the case of the 70% identical RBR paralogs *RNF19A* and *RNF19B*, this likely represents partial redundancy (Figure 1.2A, bottom). In contrast, *ARIH2*, *RBX2* (*RNF7*), and *CUL5* represent members of a single functional complex (Kelsall et al., 2013). In still other cases—for example *RNF11*, *MIB1*, and *SMURF1*—E3s cluster for reasons that are not yet understood.

Demonstrating the quality of the screen data, many compounds clustered well according to the pathways targeted. For example, thapsigargin and tunicamycin were most similar to each other, despite inducing ER stress in different ways (Figure 1.2A, bottom right). The four DNA damaging agents and the four compounds targeting the G1/S transition also clustered well. Several compounds expected to impact mitosis, either by inhibiting microtubule polymerization (colchicine and taxol) or by inhibiting the key mitotic kinases Aurora A/B and Plk1 (TAK-901 and BI-2536) clustered well with each other. Interestingly, this mitotic cluster also included the HSP70 inhibitor JG-231 (Figure 1.2A, bottom right) (Shao et al., 2018). This clustering suggests that HSP70 has one or more especially important mitotic clients. E3s whose mutation rendered cells sensitive to the mitotic cluster of inhibitors included *STUB1*/*CHIP* and *UBE4B*. STUB1 interacts with HSP70 (as well as HSP90) and its unfolded clients, whereas UBE4B interacts with

VCP/p97, and both E3s ubiquitinate client proteins to facilitate their degradation in the proteasome (Ballinger et al., 1999; Kaneko et al., 2003; Koegl et al., 1999; Meacham et al., 2001). The observation that STUB1 is sensitive to mitotic inhibitors suggests that an off-target effect of JG-231 is not responsible for its inclusion in the mitotic cluster.

The Pearson correlation coefficients of sgRNAs between replicates of each of the 41 compounds were typically very high with an average Pearson's *r* of 0.67 (Figure 1.2B & see peer-reviewed publication). Correlations between mutants in related compounds were also indicative of the quality of the screen. The G1/S cluster included four compounds. Two targeted the same kinase, CDK4/6 (palbociclib and ribociclib), one inhibited PI3K (pictilisib), and another inhibited AKT (ipatasertib), a downstream target of PI3K (Blake et al., 2012; Folkes et al., 2008; Tripathy et al., 2017). As expected, mutations that rescued or sensitized cells to the two CDK4/6 inhibitors correlated very well (Figure 1.2C). Since PI3K acts upstream of CDK4/6, but has additional downstream consequences, we expected to see a slightly weaker correlation between the screen results for pictilisib and palbociclib (Figure 1.2D). Conversely, results for compounds targeting kinases involved in distinct processes, palbociclib and the Plk1 inhibitor BI-2536 (Steegmaier et al., 2007), are not at all correlated (Figure 1.2E).

In total, our results represent 28,577 gene-compound interactions derived from over 800,000 original data points, before normalization, calculating the median of the nine sgRNAs per gene, and calculating the median of duplicates (for five compounds) or triplicates (for 36 compounds)(see peer-reviewed publication). For a gene-compound interaction to be considered valid, it had to satisfy two entirely independent stringent criteria for reproducibility and

significance. The targeting control sgRNAs (against non-expressed genes) in the 41 compounds had a mean Log2 fold change of 0.004 and a standard deviation of 0.07. We employed a cut-off greater than four standard deviations from the mean (± 0.3) for significance, along with a p-value cut-off of ≤ 0.01 for reproducibility (Figure 1.2F and 1.4C). At four standard deviations from the mean, one would expect 0.01% of our 28,577 data points (2-3) to fall outside this range by chance, and these would be very unlikely to have a p-value ≤ 0.01. Overall, we identified 466 significant and reproducibly sensitive or resistant E3/DUB-compound combinations representing about 23.7% of all genes interrogated (Figure 1.3 & 1.4A). To determine whether expression level correlated with phenotypic outcome, we compared previously reported HAP1 RNA sequencing data with our dataset and found a loose correlation (Figure 1.4B & 1.S2) (Lumb et al., 2017). Importantly, none of the 66 genes targeted by our library that are not expressed in untreated HAP1 cells showed a significant interaction with any of the 41 compounds (2,706 potential interactions), strongly validating the stringency of our cutoffs (Figure 1.4B). We conducted a parallel analysis with the MAGeCK pipeline (Li et al., 2014) and found that approximately 93% of interactions deemed significant by our initial analysis also have an FDR of 0.05 or lower (Figure 1.S7 & see peer-reviewed publication). In addition to the 466 gene-compound interactions we identified, 79 genes showed significant slow or enhanced growth in the untreated control samples, and for 27 of these, their growth was not further affected by any compound. Thus, 27.7% of all genes interrogated showed phenotypes. Many of these represent previously unreported roles of E3s and DUBs in crucial processes.

**Identification of E3s and DUBs important for growth across conditions**

Examining Log2 fold change scores for all E3 and DUB mutants in all compounds reveals both broadly important E3s/DUBs and those that appear to play much more specific roles in particular processes. For example, the mostly uncharacterized F-box protein *FBXO42* and the well-characterized F-box protein *FBXW7* are both critical for resistance to the mitotic inhibitors BI-2536 and colchicine (Figure 1.4C). However, the sensitivity of *FBXO42* mutants was quite specific to mitotic inhibition, suggesting a dedicated role in mitosis, whereas *FBXW7* mutants were sensitive or resistant to 16 of the 41 compounds. FBXW7 is a well-established tumor suppressor and substrate receptor of the SCF with numerous known substrates including cyclin E, c-JUN, MYC, and Notch (Koepp et al., 2001; Welcker and Clurman, 2008; Welcker et al., 2004).

Mutation of *MYLIP*/*IDOL*, which has been shown to ubiquitinate the LDL receptor in response to changing cellular cholesterol levels (Zelcer et al., 2009), renders cells highly sensitive to pravastatin, which inhibits HMG-CoA Reductase (Endo et al., 1976). While MYLIP was previously tied to cholesterol biology, it was not known that loss of MYLIP would cause statin sensitivity, and it was not appreciated that its role in cholesterol biology represented its key activity across the wide range of biology examined here (Figure 1.4D). In contrast, *TRIP12*, which has not previously been linked to cholesterol biology, is sensitive to both pravastatin and to several other compounds in our panel, suggesting a broader role for TRIP12. Specificity was also observed within a cluster of related compounds. For example, cells lacking *RAD18* were very sensitive to the DNA damaging agents camptothecin, cisplatin, and MMS, as expected (Figure 1.4E) (Prakash, 1981; Tateishi et al., 2000). In contrast, the mostly uncharacterized

*RNF25/AO7*, which has been suggested to have a role in NF-kB transcriptional activity (Asamitsu et al., 2003), was exquisitely sensitive to MMS in our screen, but not sensitive to other DNA damaging agents, suggesting a previously unknown, specific role in resistance to damage caused by methylation (Figure 1.4E). Closer examination of the CUL5 cluster (Figure 1.2A) reveals significant sensitivity of *CUL5*, *RBX2* (*RNF7*), *ARIH2*, and a potential substrate receptor *WSB2* to the CRM1 inhibitor leptomycin B (Kudo et al., 1999), suggesting a function that is critical when nuclear export is compromised (Figure 1.4F). Mutation of three core components, *CUL5*, *RBX2*, and *ARIH2*, also caused resistance to the G1/S inhibitors. However, *WSB2* mutation did not cause significant resistance to these compounds, suggesting that an alternate substrate receptor(s) may be responsible for this G1/S phenotype. The cluster of the RBR paralogs *RNF19A* and *RNF19B* showed a striking sensitivity to the mitotic inhibitor cluster, which is mirrored by resistance of cells with sgRNAs targeting *SMURF1* (as well as *RNF11* and *MIB1*) to the same inhibitors (Figure 1.4G). Despite their 70% sequence identity, RNF19A and RNF19B have been reported to play roles in distinct processes: clearance of aggregates in Lewy bodies and innate immunity, respectively (Fortier and Kornbluth, 2006; Ito et al., 2003). Our data instead suggest that these E3s have highly related functions. The HECT E3 SMURF1 has been shown to regulate the BMP/TGF-β signaling pathway, as well as cell migration via ubiquitination of RhoA (Wang et al., 2003; Zhu et al., 1999). Our data are consistent with the regulation of RhoA by SMURF1 extending to the role of RhoA in the contractile ring during cytokinesis.

In addition to the novel mitotic sensitivity of *FBXO42* that we observed, *HUWE1* and *UBE3D* were also sensitive to the cluster of mitotic inhibitors (Figure 1.4H). The massive 480 kDa

HECT E3 HUWE1 has numerous reported roles, most notably in the DNA damage response and apoptosis, but has not been directly linked to mitosis (Hall et al., 2007; Zhong et al., 2005). UBE3D, also a HECT E3, has no confirmed function *in vivo*.

**Validation of observed sensitivities and resistances**

To independently validate our screen results, we developed an internally controlled, two color competitive growth assay. Briefly, in quadruplicate, inducible $Cas9^+$ $GFP^+$ HAP1 cells were mixed with $BFP^+$ HAP1 cells, infected with a mini-pool of two to four sgRNAs targeting one gene, and then split into media with or without compound every two days for eight days, with the GFP/BFP ratio being measured by flow cytometry (Figure 1.5A and Supplementary File 1.S4). Data were normalized to the day zero GFP/BFP ratio, then to the matched untreated GFP/BFP ratios for each time point to normalize out growth defects. A control experiment with a pool of 11 targeting control sgRNAs showed that Cas9 cutting alone did not render the $Cas9^+$ $GFP^+$ cells significantly sensitive to these compounds (Figure 1.5B). Next, we repeated the experiment in parallel with 15 different sgRNA mini-pools to validate E3/DUB interactions: *DCAF7*, *TRIM28*, *FBXW7*, *BIRC6* (palbociclib sensitive/resistant); *RNF25*, *USP34*, *RAD18* (DNA damage sensitive); *HERC2*, *UBE4B* (CB-5083 and/or cytochalasin D sensitive); *ZBTB11*, *LTN1* (cycloheximide resistant/sensitive); *KEAP1* (tanespimycin sensitive); *MYLIP* (Pravastatin sensitive); *SYVN1* (thapsigargin sensitive); and *FBXO8* (brefeldin A resistant) (Figure 1.5C-Q). Cytochalasin D served as a negative control for all but two experiments; in the screen data, and recapitulated in the GFP/BFP assay, *HERC2* and *UBE4B* showed significant (Log2 of -0.68) and moderate (Log2 of -0.19) sensitivity to cytochalasin D, respectively. This assay did not reproduce the observed sensitivity of *TRAF2* and *ZBTB7A* to the CDK9 inhibitor flavopiridol

(data not shown), perhaps due to the difficulty in dosing this inhibitor. Overall, the results of the independent validation experiments suggest that the dataset is highly reproducible.

To test whether the sensitivity to mitotic inhibitors observed with mutation of certain E3s is associated with novel mitotic roles, we generated 1-2 clonal mutants each of *FBXO42*, *HUWE1*, *UBE3D*, *HERC2*, *UBE4B*, and *RNF19A* in HAP1-Cas9 cells. All mutant clones were screened by Sanger sequencing and by western blot when antibodies were available (Figure 1.S3A & 1.S3B). For each clone, we performed internally controlled, competitive growth assays with HAP1-WT-GFP$^+$ cells with and without inhibitors (Figure 1.6A). As with the GFP/BFP validation assay, data were normalized to the day zero GFP+/– ratios, then normalized to the matched untreated GFP+/– ratios for each time point, and cytochalasin D served as a negative control compound for most experiments. We found *FBXO42*, *HUWE1*, and *UBE3D* mutant clones to be sensitive to two or more of the mitotic inhibitors BI-2536 (Plk1), colchicine (microtubules), and TAK-901 (Aurora A/B) (Figure 1.6B-D). The screen results did not identify *HUWE1* as sensitive to DNA damaging agents (Figure 1.4H), but given the previously reported role of HUWE1 in the DNA damage response, we sought to more rigorously test whether this was the case with our clonal mutants of *HUWE1*. In this assay, we observed a subtle sensitivity to the Topoisomerase I inhibitor camptothecin (Figure 1.6C). This suggests, at least in HAP1 cells and across the pathways we interrogated, that the more critical role of HUWE1 may be in mitosis.

The GFP+/– assay with clonal *HERC2* mutant cells confirmed sensitivity to the mitotic inhibitors (Figure 1.6E). Additionally, *HERC2* was the most sensitive of all genes interrogated to the actin

polymerization inhibitor cytochalasin D (Figure 1.3), and this was also apparent in clonal mutants in the GFP+/– assay (Figure 1.6E). Intriguingly, the strong sensitivity of *HERC2* mutant cells to both cytochalasin D and the Plk1 inhibitor BI-2536 may be related to the reported physical interaction between HERC2 and the actin regulator srGAP2 and may lend support to the proposed role of HERC2 in centrosome maturation via ubiquitination of NEURL4 (Al-Hakim et al., 2012). HERC2 is thought to play a role in the DNA damage response by promoting histone ubiquitination by RNF8 as well as positively regulating RNF168, although research in chicken cells suggests that HERC2 is dispensable for the activity of RNF8 and RNF168 (Bekker-Jensen et al., 2010; Oestergaard et al., 2012). We saw no de-enrichment of *HERC2* sgRNAs when cells were subjected to DNA damaging agents in our screen. Coupled with the competitive growth assay results in mitotic inhibitors (Figure 1.6E), the most critical roles of HERC2 may be in the cytoskeleton and mitosis.

*UBE4B* has a well-established association with VCP/p97 and ubiquitin chain elongation (Kaneko et al., 2003; Koegl et al., 1999). Consistently, *UBE4B* mutants displayed the strongest sensitivity to the VCP/p97 inhibitor CB-5083 (Figure 1.3), and this effect was also observed in the GFP+/– assay (Figure 1.6F). UBE4B has been shown to be highly phosphorylated in mitosis and its knockdown results in mitotic delays and numerous mitotic abnormalities (Spinette et al., 2004). The results of the screen and validation with clonal *UBE4B* mutant cells shown here provide confirmation of a role of UBE4B in mitosis. It is unclear why the modest cytochalasin D sensitivity seen in the pooled GFP/BFP assay for UBE4B (Figure 1.5N) was not observed in the clonal GFP+/– assay. Finally, *RNF19A* mutant clones displayed variable results in the GFP+/–

assay, with a subset of clones showing sensitivity to the mitotic inhibitors, perhaps due to suppressors arising (data not shown).

To test whether the E3s that we validated in HAP1 cells recapitulated in another cell line, we generated pools of the osteosarcoma cell line U2OS expressing a constitutive shRNA against a subset of E3s. We chose E3s whose deletion causes resistance, as these phenotypes are more robust than sensitivities due to their continued outgrowth of the control population. In GFP+/- competitive growth assays, FBXW7, BIRC6, and FBXO8 recapitulated the resistances observed in HAP1 (Figures 1.6G-I & Figures 1.S6A-1.S6B). ZBTB11 knockdown did not show the expected resistance to cycloheximide (Figure 1.6J & 1.S6C), and it is possible that complete loss of ZBTB11 is required to observe resistance.

**FBXO42, HUWE1, and UBE3D play important roles in mitosis**

To determine why mutation of *FBXO42*, *HUWE1*, or *UBE3D* rendered cells sensitive to inhibitors of mitosis, we tested how the cell cycle was affected in these mutants. *HUWE1* and *UBE3D* clonal mutant cells grown in moderate doses of BI-2536 or colchicine for 24 hours displayed a significant accumulation at a G2/M DNA content by propidium iodide staining as compared to wild type controls (Figures 1.7A-1.7C). Inhibition of Aurora A/B with TAK-901 had a different effect on the clonal deletes: after 10 hours, cells accumulated at a G2/M DNA content (Figure 1.7E), and after 24 hours, cells accumulated at a G2/M polyploid DNA content, suggesting a failure to complete cytokinesis (Figures 1.7D & 1.7F). While TAK-901 has been previously reported to induce polyploidy by blocking Aurora B-dependent cytokinesis (Farrell et

al., 2013; Schumacher et al., 1998), mutation of *HUWE1* or *UBE3D* significantly enhanced this defect compared to wild type cells.

Since propidium iodide staining does not examine cell cycle position directly, but instead only measures DNA content, we assessed these mutants by immunofluorescence microscopy. We treated wild type, *HUWE1*, *UBE3D*, and *FBXO42* clonal mutants with a moderate dose of BI-2536 for 24 hours and processed them for α-tubulin immunofluorescence (Figure 1.7G). We found that a moderate dose of BI-2536 that had little effect on wildtype cells caused a significant mitotic accumulation in *HUWE1*, *UBE3D*, and *FBXO42* mutant clones (Figure 1.7G, and 1.7H, top). It has been previously shown that BI-2536-treated cells accumulate monopolar spindles, circled by a ring of chromosomes (Figure 1.7G, right) (Steegmaier et al., 2007). We quantified the frequency of monopolar spindles upon BI-2536 treatment and observed a 6 to 9-fold increase over wildtype in *HUWE1*, *UBE3D*, and *FBXO42* mutants (Figure 1.7H, bottom). Other aberrant spindle morphologies were also observed at very low frequencies in wild type cells and mutants, with and without the inhibitor (data not shown). Importantly, in unperturbed cells, we also observed a 5 to 7-fold increase of monopolar spindles in *HUWE1*, *UBE3D*, and *FBXO42* mutants (Figure 1.7H, bottom). These results suggest that *HUWE1*, *UBE3D*, and *FBXO42* promote the formation of a bilateral spindle during normal cell division.

**The mitotic role of FBXO42 is conserved in cells from a distinct lineage**

As HUWE1 and UBE3D are cell essential in many cell lines while FBXO42 is not, we focused on FBXO42 going forward. To test whether FBXO42 plays a similar mitotic role in another cell line, we generated stable pools of cells expressing one of two shRNAs against *FBXO42*, or a

control shRNA, in U2OS cells. We combined these $GFP^-$ cells expressing *FBXO42* or control shRNAs with $GFP^+$ U2OS cells (also expressing the control shRNA), and examined the ratio of $GFP^+$ to $GFP^-$ cells, as in Figure 1.6, as these cells were passaged in the presence of BI-2536, colchicine, TAK-901, or left untreated. As in HAP1, U2OS cells depleted of FBXO42 displayed significant sensitivity to the mitotic inhibitors (Figure 1.8A, 1.8B, 1.S4A). Using the same shRNA pools, we measured the cell cycle distribution of FBXO42-depleted and control U2OS cells by propidium iodide staining in the presence of a moderate dose of TAK-901 and found that FBXO42 knockdown resulted in significant accumulation of cells with a G2/M content, suggesting an important mitotic role of FBXO42 (Figure 1.8C, 1.S4B, 1.S4C, 1.S4D).

We also examined the effect of BI-2536 treatment on U2OS cells depleted of FBXO42 by immunofluorescence microscopy, and we observed a significant increase of monopolar spindles in FBXO42-depeleted U2OS cells after 24 hours of treatment with a low dose of BI-2536 for each of the two FBXO42 shRNAs used (Figure 1.8D & 1.8E). Very low frequencies of other aberrant spindle morphologies were also observed in wild type cells and FBXO42-depleted cells both in the absence and the presence of the inhibitor (data not shown). Taken together, our results show that FBXO42 performs a similar mitotic role in both HAP1 and U2OS cells.

## DISCUSSION

With over 600 members, the human E3 family is larger than the kinome and represents a significant and diverse mode of regulation that impacts nearly all areas of biology. Comprehensive efforts to identify E3 substrates and ubiquitination sites have aided the effort to characterize all components of the UPS and its targets (Benanti et al., 2007; Bennett et al., 2010; Komander and Rape, 2012; Loveless et al., 2015; Mark et al., 2014; Rose et al., 2016; Yen and Elledge, 2008). However, substrates are often difficult to detect, and it is hard to systematically ascertain whether the loss of any of these individual ubiquitination events is phenotypic. With the advent of CRISPR-Cas9 technology, high-throughput genetic analysis in human cells is now possible, and we applied this approach to systematically probe the human E3s and DUBs for involvement in a broad range of biological processes. By combining gene mutations with 41 compounds targeting numerous processes, we were not only able to determine the importance of each E3 and DUB under stress conditions, but also to compare results across our dataset to determine the relative specificity of each effect. We found numerous novel interactions that represent promising areas for future research, including a previously unknown crucial mitotic role for the substrate receptor FBXO42.

Broad analysis of our screen dataset reveals several revelatory themes related to E3 modularity. The largest single class of E3s, the cullin-RING ligases (CRLs), consist of core components (e.g. CUL1, RBX1) and modular substrate receptors (SRs), with each cullin having dozens to over a hundred different SRs. Some CRL subunits, such as CUL1, RBX1, and ANAPC11, have many essential functions and SRs, and therefore cells lacking these functions dropped out of the population so quickly that we were unable to detect any compound-specific

interactions in our screen. In contrast to CUL1, we did see specific interactions for CUL2, CUL3, CUL4A, CUL4B, and CUL5 (Figure 1.S5). The CUL4A and CUL4B data were highly correlated (Pearson corr. coef. = 0.7), although CUL4A showed stronger phenotypes (Figure 1.S5A). Both *CUL3* and its SR *KEAP1* were the most sensitive of all genes interrogated to the HSP90 inhibitor tanespimycin (Kasai et al., 2016) (Figure 1.3, 1.S5B). CUL2 and CUL5 appear to have overlap in SRs, making it hard to determine which SRs function primarily with which cullin. Three core components of a CUL5 complex, *CUL5, RBX2*, and *ARIH2* were strongly sensitive to inhibition of nuclear export with leptomycin B, and were resistant to inhibitors of CDK4/6 and PI3K (Figure 1.3, 1.4F, 1.S5C). A putative SR for this complex, *WSB2*, was specifically sensitive to leptomycin B and not significantly responsive to the G1/S inhibitors, suggesting it works with CUL5 and may be the main SR responsible for the sensitivity of the complex to inhibition of nuclear export. There is likely another SR or SRs responsible for the observed resistance of the core complex to inhibitors of the G1/S transition. CUL5 was sensitive to the cellular respiration inhibitor TTFA, whereas CUL2 showed resistance. The SR SOCS4 and adapter TCEB3 both showed strong resistance to this compound, suggesting that SOCS4 and TCEB3 function with CUL2 to affect this response. In cases where no single SR could account for a resistance or sensitivity seen in the cullin, it is likely that multiple SRs contribute to the effect.

The genetic rescues in our dataset fell into two broad categories: mutants that were truly resistant to a particular compound and those whose negative effect on cell growth was rescued by a particular compound (Figure 1.1F). In general, cytotoxic compounds such as BI-2536 (Plk1) predominantly revealed true resistance, while cytostatic compounds such as cycloheximide

(translation) identified many slow growing mutants that were rescued by the drug (Figure 1.3). Truly resistant mutants are more likely to be examples of specific, on-pathway suppression, whereas general suppression is likely to occur with cytostatic compounds. For example, *VPS11*, *VPS18*, and *VPS41*, which are part of the HOPS complex and regulate endocytosis by promoting vesicle fusion with endosomes (Brocker et al., 2012; Lin et al., 2014; Segala et al., 2019), were truly resistant to pravastatin, whereas *VPS18* loss was rescued by treatment with palbociclib (Figure 1.3). *VPS41* mutation also rescued brefeldin A treatment, possibly because reducing flux through the endocytic pathway by deleting components of the HOPS complex maintains proteins at the plasma membrane.

Among the genetic rescues we observed in our dataset, there were many reasons for resistance that can be explained by the molecular activity of the deleted E3. Mutation of *FBXW7* rendered cells strongly resistant to inhibitors of CDK4/6 and PI3K. Because FBXW7 promotes ubiquitination and degradation of MYC and cyclin E, FBXW7 has the overall effect of inhibiting the G1/S transition (Koepp et al., 2001; Moberg et al., 2001; Strohmaier et al., 2001; Welcker et al., 2004). Therefore, mutating *FBXW7* may make cells resistant to chemical inhibitors of the G1/S transition by boosting levels of proteins that promote that transition, such as MYC and cyclin E. *ZNF598* mutants likely displayed resistance to cycloheximide for a very different reason. ZNF598 ubiquitinates several ribosomal proteins in response to ribosome stalling, and this ubiquitination leads to dissociation of the 40S and 60S ribosomal subunits and recruitment of LTN1, ultimately enabling recycling of the ribosomal subunits and clearance of nascent, potentially aberrant polypeptides (Juszkiewicz and Hegde, 2017; Juszkiewicz et al., 2018; Sundaramoorthy et al., 2017). In the presence of the translation elongation inhibitor

cycloheximide, global translation is slowed. Deleting *ZNF598* may enable this impaired translation to continue, without the QC pathway detecting all slowed ribosomes as terminally stalled. In contrast, LTN1, which ubiquitinates nascent polypeptides in the exit tunnel of the ribosome, is sensitive to cycloheximide. This is likely because LTN1 acts after translation has already been disrupted, thereby allowing ribosomal recycling (Brandman et al., 2012).

There are several potential reasons for synthetic sensitivity. For example, the sensitivity of *WSB2* to the CRM1 inhibitor leptomycin B may be through direct involvement with nuclear export or because it is important for some process that makes nuclear export critical, such as nuclear integrity. Unbiased clustering revealed that *RNF11*, *MIB1*, and *SMURF1* all rescue mitotic inhibition. Again, this could represent a direct or secondary effect on mitosis. These three E3s are all reported to localize to the plasma membrane, at least in part, but each has a different function in regulating intracellular sorting, differentiation, and cell motility and polarity, respectively (Itoh et al., 2003; Santonico et al., 2015; Wang et al., 2003; Zhu et al., 1999). Our data suggest a previously unknown potential overlap in function of RNF11, MIB1, and SMURF1 and warrants further study. Importantly, while some of these chemical-genetic interactions may not be direct, they are not likely to be due to entirely pleiotropic phenotypes caused by a general effect on apoptosis, transcription, translation, or other housekeeping activities, as this would be unlikely to yield specific sensitivities. Moreover, a general effect on a basic biological process would almost surely cause a particularly strong negative interaction when that process is directly inhibited.

Our systematic screening of the UPS revealed numerous gene-compound interactions. Mutation of the uncharacterized F-box protein *FBXO8* renders cells resistant to the vesicular transport inhibitor brefeldin A, consistent with the presence of a Sec7-like domain in *FBXO8* (Esmon et al., 1981; Misumi et al., 1986; Stevens et al., 1982). We find that loss of the poorly studied E3 RNF25 causes cells to be exquisitely sensitive to MMS (Figure 1.3 & 1.4E), suggesting a role for RNF25 in detection or repair of methylation-induced damage. Because *RNF25* was not sensitive to other DNA damaging agents, we hypothesize a specific role for RNF25 in surviving methylation damage. In contrast, well-established DNA repair factors such as RAD18 and FANCL were required for cell survival upon exposure to several different types of damaging agents. Interestingly, loss of the DUB USP34 also caused strong MMS sensitivity (Figure 1.3 & 1.5I). Like many poorly characterized genes, USP34 has been placed in several pathways. Single studies have implicated USP34 in cell migration, cell survival, BMP signaling, heart disease, EMT and stem cell maintenance, NF-kB and Wnt signaling, and the DNA damage response (Guo et al., 2018; Lin et al., 2020; Lui et al., 2011; Oh et al., 2017; Sy et al., 2013). Thus, while many genes have been suggested to have associations with the DNA damage response, our unbiased approach helps to identify those, like USP34, that have significant and specific roles in this area of biology.

Our screen uncovered a previously unknown role of the F-box protein FBXO42, as well as HUWE1 and UBE3D, in faithful completion of mitosis. Although one report suggested that UBE3D is capable of ubiquitinating cyclin B *in vitro* (Kobirumaki et al., 2005), no *in vivo* role for UBE3D in this, or any other process, has been reported, and the APC/C has a well-established role in cyclin B turnover (Sudakin et al., 1995). Numerous roles for HUWE1 have

been reported, such as involvement in the DNA damage response and regulation of apoptosis, so future work is required to determine the extent of HUWE1 involvement in mitosis (Hall et al., 2007; Zhong et al., 2005). In our hands, and as reported in numerous genome-wide studies, *HUWE1* and *UBE3D* appear to be cell essential in many other cell lines, which may have allowed their mitotic roles to go unnoticed. As part of an SCF complex, FBXO42 has been implicated in ubiquitination and degradation of p53 (Sun et al., 2009). However, this function is likely to be highly redundant, given other well-established E3s, such as MDM2, in this process (Lane et al., 2010). Unlike *HUWE1*, *UBE3D*, *HERC2* and *UBE4B*, *FBXO42* mutants showed no sensitivity to any other agents used, in either our screen data or our subsequent follow-up experiments. Not only does removal of *FBXO42* in HAP1 and U2OS cells cause sensitivity to various inhibitors of mitosis and the accumulation of monopolar spindles, but knockdown of *FBXO42* in U2OS cells in the presence of a low dose of a mitotic inhibitor results in accumulation of cells with a G2/M DNA content. Lending further support for an important cell growth role of FBXO42, a genome-wide screen of tumors derived from glioblastoma stem-like cells found that some isolates were strongly dependent on FBXO42 for growth, whereas non-neoplastic controls were not (Toledo et al., 2015). Interestingly, other genes identified in this same screen are involved in mitosis, and unpublished data from the Paddison laboratory shows that FBXO42 is required for mitotic progression in GSC-0827 cells (Hoellerbauer and Paddison, personal communication). Collectively, these data suggest that FBXO42 performs a mitotic role in many cell types, but that role may only be essential in a subset of cell types depending upon the expression of other mitotic genes.

Our screen identified phenotypes for over 27% of the E3s and DUBs interrogated. About 10% of the E3s/DUBs in our library are not expressed in HAP1 cells (Lumb et al., 2017), and about one third are very poorly expressed, although this may vary after treatment with particular compounds. It is possible that these genes are more important in cell lines from other lineages or at specific stages of development. Alternatively, they may be critical for areas of biology not covered in our screen, such as the response to pathogens. Additionally, it is well-established that many ubiquitinated proteins are redundantly targeted by two or more E3s (Koren et al., 2018). Now that effective methods for double mutant genetic interaction mapping using CRISPR-Cas9 have been developed, we predict that many more E3 and DUB functions will be uncovered by applying these methods to the UPS (Horlbeck et al., 2018). While synthetic genetic analysis is a useful strategy, the systematic chemical-genetic approach employed here has the distinct advantage that the level of inhibition of a pathway can be precisely controlled, whereas the proteins functioning within those pathways may be either cell essential or fully redundant. Thus, our work represents both a valuable resource to those studying the UPS and an important starting point to investigate other biological pathways.

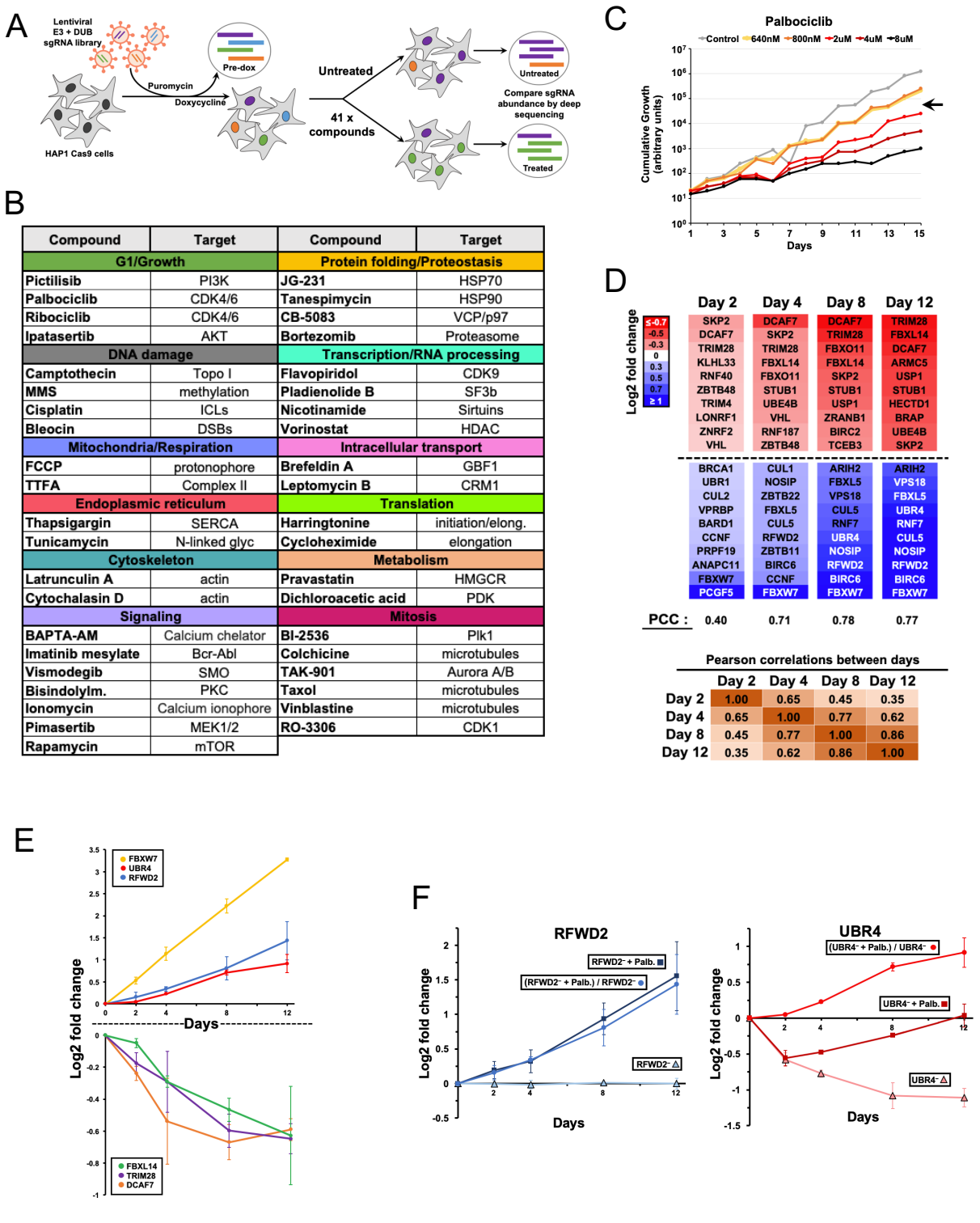


| Compound | Target | Compound | Target |
|---|---|---|---|
| **G1/Growth** | | **Protein folding/Proteostasis** | |
| Pictilisib | PI3K | JG-231 | HSP70 |
| Palbociclib | CDK4/6 | Tanespimycin | HSP90 |
| Ribociclib | CDK4/6 | CB-5083 | VCP/p97 |
| Ipatasertib | AKT | Bortezomib | Proteasome |
| **DNA damage** | | **Transcription/RNA processing** | |
| Camptothecin | Topo I | Flavopiridol | CDK9 |
| MMS | methylation | Pladienolide B | SF3b |
| Cisplatin | ICLs | Nicotinamide | Sirtuins |
| Bleocin | DSBs | Vorinostat | HDAC |
| **Mitochondria/Respiration** | | **Intracellular transport** | |
| FCCP | protonophore | Brefeldin A | GBF1 |
| TTFA | Complex II | Leptomycin B | CRM1 |
| **Endoplasmic reticulum** | | **Translation** | |
| Thapsigargin | SERCA | Harringtonine | initiation/elong. |
| Tunicamycin | N-linked glyc | Cycloheximide | elongation |
| **Cytoskeleton** | | **Metabolism** | |
| Latrunculin A | actin | Pravastatin | HMGCR |
| Cytochalasin D | actin | Dichloroacetic acid | PDK |
| **Signaling** | | **Mitosis** | |
| BAPTA-AM | Calcium chelator | BI-2536 | Plk1 |
| Imatinib mesylate | Bcr-Abl | Colchicine | microtubules |
| Vismodegib | SMO | TAK-901 | Aurora A/B |
| Bisindolylm. | PKC | Taxol | microtubules |
| Ionomycin | Calcium ionophore | Vinblastine | microtubules |
| Pimasertib | MEK1/2 | RO-3306 | CDK1 |
| Rapamycin | mTOR | | |

**Figure 1.1. CRISPR-Cas9 screen of the ubiquitin pathway.**

**(A)** Overview of the E3/DUB CRISPR-Cas9 screening approach. Three independently generated doxycycline-inducible Cas9-expressing HAP1 clones were infected at an MOI of approximately 0.4 with a custom E3 and DUB sgRNA library. After selecting for sgRNA

integration for four days and induction of Cas9 expression for three days, cells were split into media with or without one of 41 different compounds. Every two days, cells were split into fresh compounds. After eight days, cells were harvested, sgRNAs were sequenced, and relative sgRNA abundance was determined. Pre-dox samples were also collected (pre-Cas9 induction). Throughout the experiment, approximately 1,000-fold coverage of each sgRNA was maintained when splitting and sequencing.

**(B)** The 41 chemical compounds used in the CRISPR-Cas9 screen, showing the primary target or effect of each compound. DSBs = double strand breaks; ICLs = DNA interstrand crosslinks.

**(C)** Palbociclib dose selection for the screen. A dose that inhibited apparent growth to about 70% of untreated controls was selected. Cumulative growth is reported in arbitrary units and is based on observations of cell confluency.

**(D)** Eight days in 1.5μM palbociclib was sufficient to uncover reproducible sensitivities and resistances. Data were normalized to untreated samples, and the ten most enriched and de-enriched genes are shown as Log2(treated/untreated). Pearson correlation coefficients (PCC) between repeats carried out in two independent HAP1-Cas9 clones are shown, as are PCCs between days.

**(E)** Three sensitive and three resistant E3 mutants in palbociclib. As in (D), each time point was done in duplicate, and data were normalized to untreated samples. Data plotted as mean ± SEM.

**(F)** Comparison of un-normalized data (triangles and squares) vs. normalized data (circles) distinguishes between compounds that rescue slow growing mutants (e.g. *UBR4* in red) and mutations that confer true resistance to a compound (e.g. *RFWD2* in blue). Normalized data represent the Log2(palbociclib treated/untreated). As in (D), each time point was done in duplicate. Data plotted as mean ± SEM.

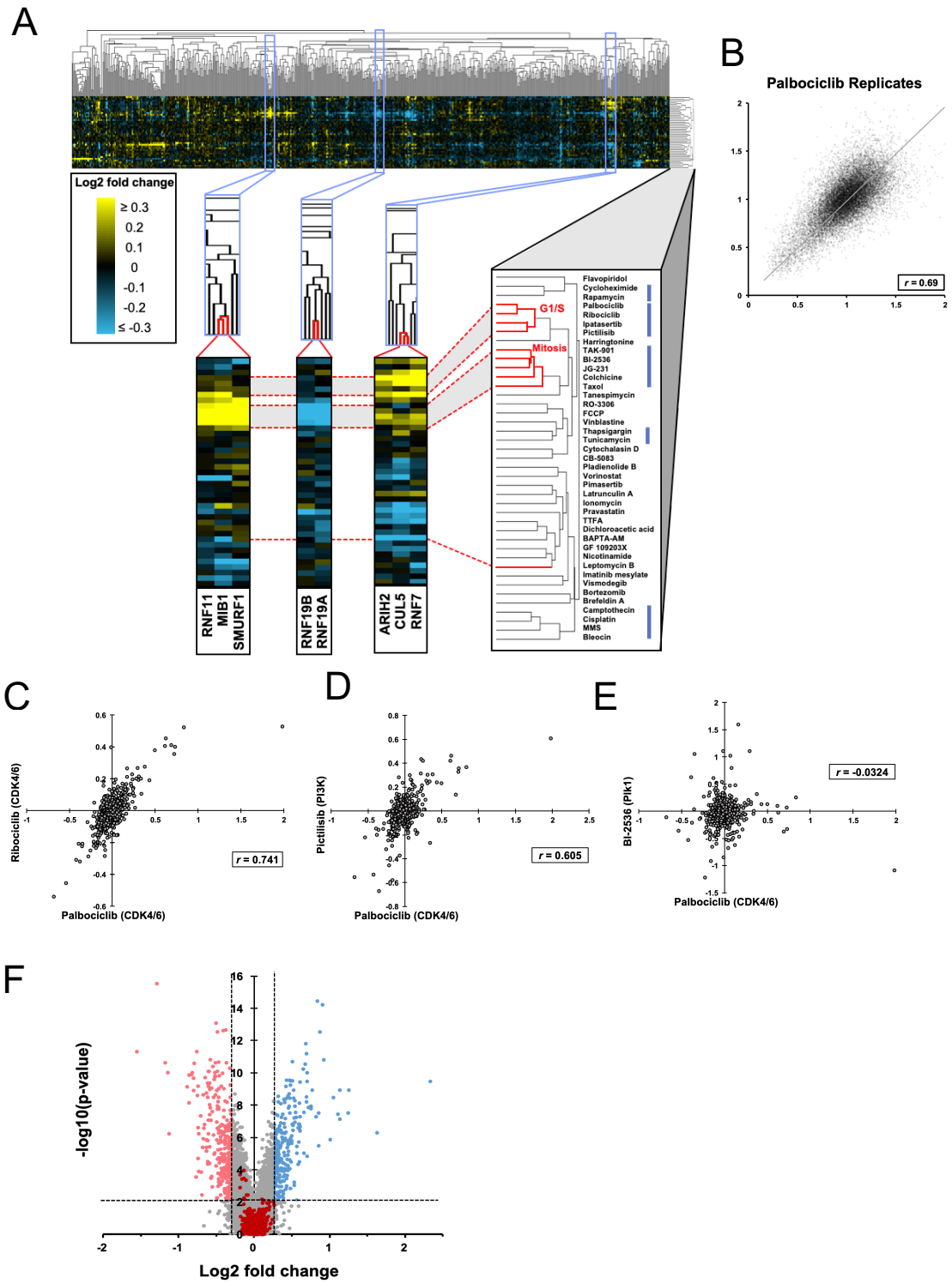


**Figure 1.2. Mapping ubiquitin ligase and DUB roles across fundamental biological processes.**

**(A) Top**: a quantitative chemical-genetic map showing average linkage unbiased hierarchical clustering of genes (along the top) and compounds (along the right side) based on Log2 fold

change of sgRNAs. Data represent three independent replicates which were normalized to untreated controls. Blue pixels represent combinations that grew less well than untreated controls (sensitive), black pixels represent no change, and yellow pixels represent combinations that grew better than untreated controls (resistant). **Bottom right:** detail of compound clustering, e.g.: G1 inhibitors; mitotic inhibitors; ER stress inducers; and DNA damaging agents (lavender bars). **Bottom left:** Example gene clusters: A CUL5 CRL complex; 70% identical RBR paralogs RNF19A and RNF19B; and MIB1, SMURF1, and RNF11.

**(B)** Pearson correlation between the three palbociclib replicates. Data were normalized to pre-dox samples. Each point represents one sgRNA. 99.76% of points are displayed.

**(C)** Data for two different inhibitors of CDK4/6, ribociclib vs. palbociclib.

**(D)** Data for inhibitors of two different G1/growth factors, pictilisib (PI3K) vs. palbociclib (CDK4/6).

**(E)** Data for inhibitors of unrelated processes, BI-2536 (Plk1) vs. palbociclib (CDK4/6).

**(C-E)** Each data point represents the Log2 fold change of a single gene, calculated from the median of three replicates normalized to untreated controls. Pearson's correlation coefficients (*r*) are shown.

**(F)** Volcano plot of Log2 fold change vs. –Log10(p-value) for 697 genes over 41 conditions (28,577 total data points). Targeting and non-targeting control genes (656 points) are depicted in dark red. Log2 fold change cut-offs of 0.3 and -0.3 were determined by calculating four standard deviations from the mean of the targeting control sgRNAs. A stringent –Log10(p-value) cut-off of 2 was selected (p-value $\leq$ 0.01).

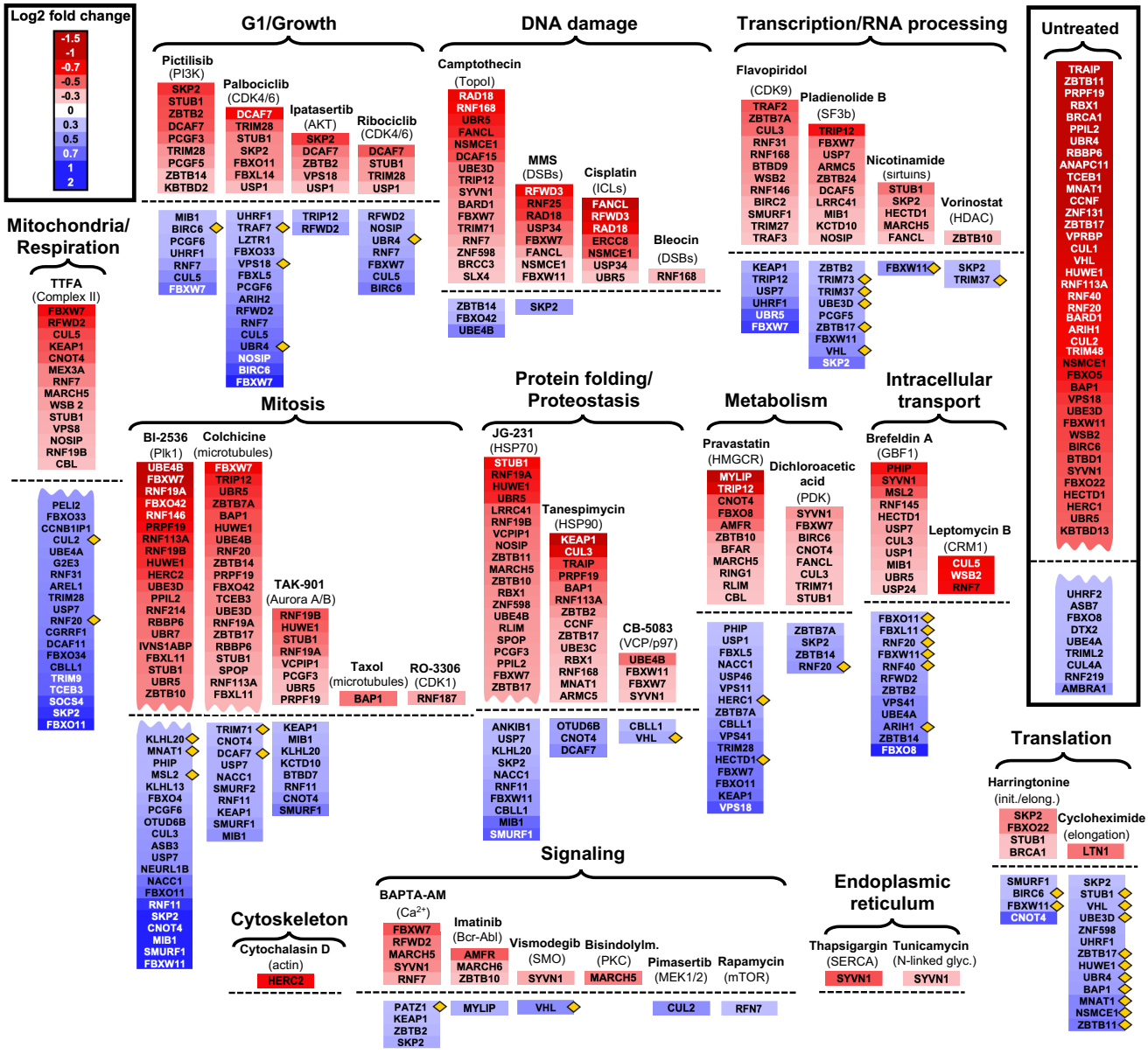


**Figure 1.3. Chemical-genetic map identifies roles of numerous previously unknown ubiquitin ligases and DUBs.**

Data represent the median of replicates, normalized to untreated controls. As in Figure 1.2F, E3s and DUBs listed here fulfill two criteria: (1) post-normalization Log2 fold change ≤ -0.3 or ≥ 0.3, AND (2) –Log10(p-value) ≥ 2. For brevity, lists longer than 20 genes have been truncated, indicated by jagged lines. For the complete list see peer-reviewed publication. For five of the 41 compounds, no genes fulfilled the two criteria. Apparently resistant E3/DUB mutants that are instead partially rescued by the inhibitor are indicated by a yellow diamond (e.g. *UBR4* in Figure 1.1F). Untreated data on the right shows the 40 slowest growing and nine most enriched genes. These have been normalized to pre-dox samples, not to untreated, and represent the median of 15 replicates.

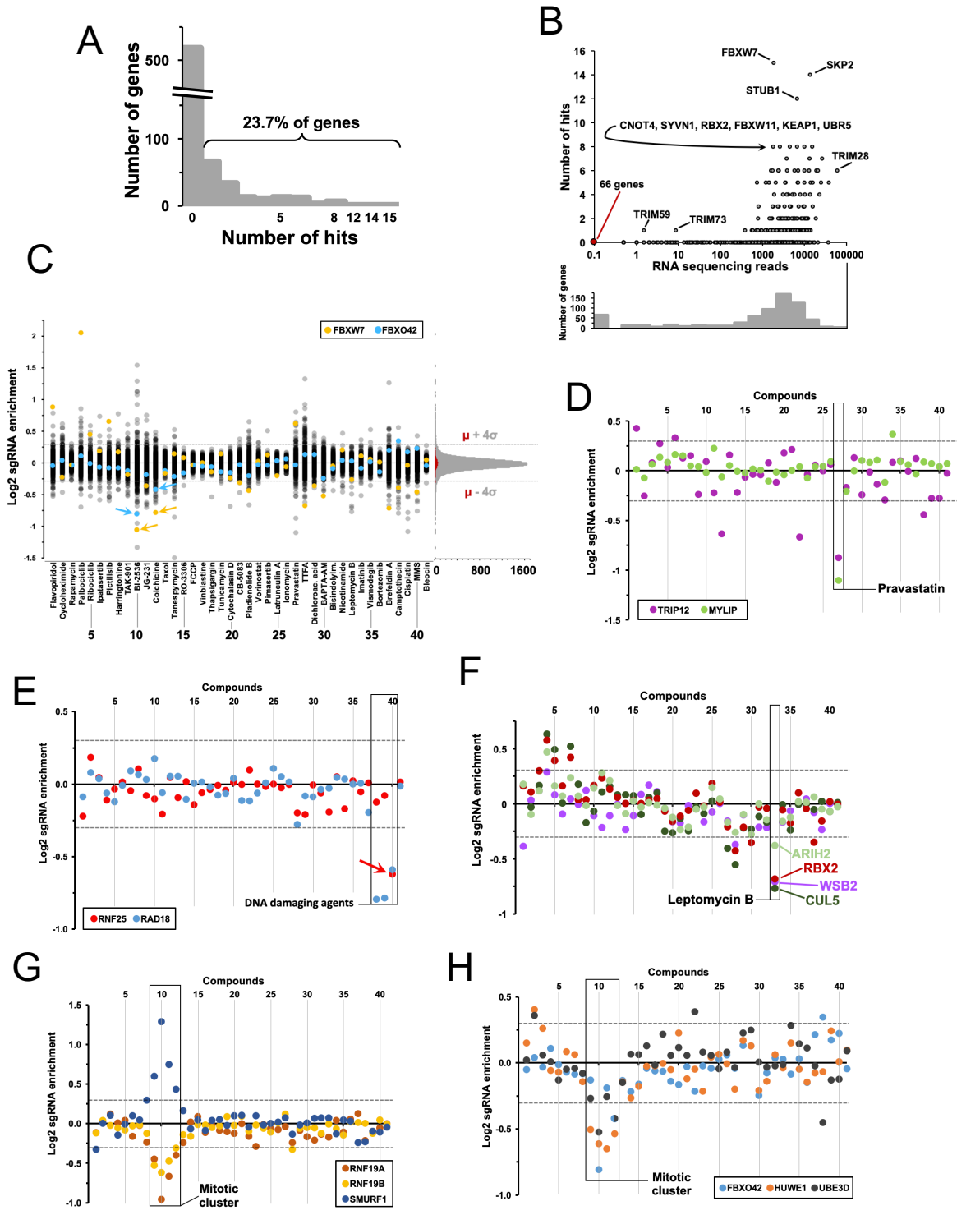


**Figure 1.4. Chemical-genetic map identifies roles of numerous previously unknown ubiquitin ligases and DUBs.**

**(A)** 23.7% of genes were significantly and reproducibly sensitive or resistant to one or more of the 41 inhibitors tested (using the same criteria as in Figure 1.3).

**(B)** **Top:** Correlation between the number of times a gene was significantly and reproducibly sensitive or resistant to a compound (using the same criteria as in Figure 1.3) and gene expression. RNA sequencing data are the average of two replicates of WT untreated HAP1 cells, raw sequencing reads (data from Lumb et al., 2017). For the purposes of this plot, genes with no detected sequencing reads were set to 0.1. **Bottom:** Histogram of the number of genes in each RNA sequencing read bin.

**(C)** Log2 fold change scores for each compound reveal genes with specific and non-specific interactions. *FBXW7* (yellow) falls above the Log2 fold change cut-off in 16 compounds. Conversely, *FBXO42* (blue) is more specific and only falls above the cut-off in three compounds. **Right:** histogram of number of genes at each Log2 fold change score with a bin size of 0.01. Targeting control genes depicted in red (with a range of -0.29 to +0.24). Dashed lines indicate four standard deviations from the mean of the targeting control sgRNAs and should contain 99.99% of negative results.

**(D)** Log2 fold change scores of *MYLIP* (green) and *TRIP12* (purple) in 41 compounds show the relatively specific sensitivity of *MYLIP* to HMGCR inhibitor pravastatin compared to the more broadly sensitive *TRIP12*.

**(E)** Log2 fold change scores of *RAD18* (blue) and *RNF25* (red) in 41 compounds show that *RAD18* is sensitive to several DNA damaging agents while *RNF25* is specifically sensitive to MMS.

**(F)** Log2 fold change scores of *ARIH2*, *CUL5*, *RBX2* (*RNF7*), and *WSB2* in 41 compounds show the sensitivity of this putative CRL complex to the CRM1 inhibitor leptomycin B.

**(G)** Log2 fold change scores of *SMURF1* and paralogs *RNF19A* and *RNF19B* in 41 compounds show inverse responses to several mitotic inhibitors.

**(H)** Log2 fold change scores of *FBXO42*, *HUWE1*, and *UBE3D* in 41 compounds show sensitivity to several mitotic inhibitors. *FBXO42* and *UBE3D* have the same Log2 fold change (-0.42) for the fourth mitotic inhibitor colchicine (compound #12), indicated by bisected data point.

**(D-H)** Compounds 1-41 in the same order as in Figure 1.4C.

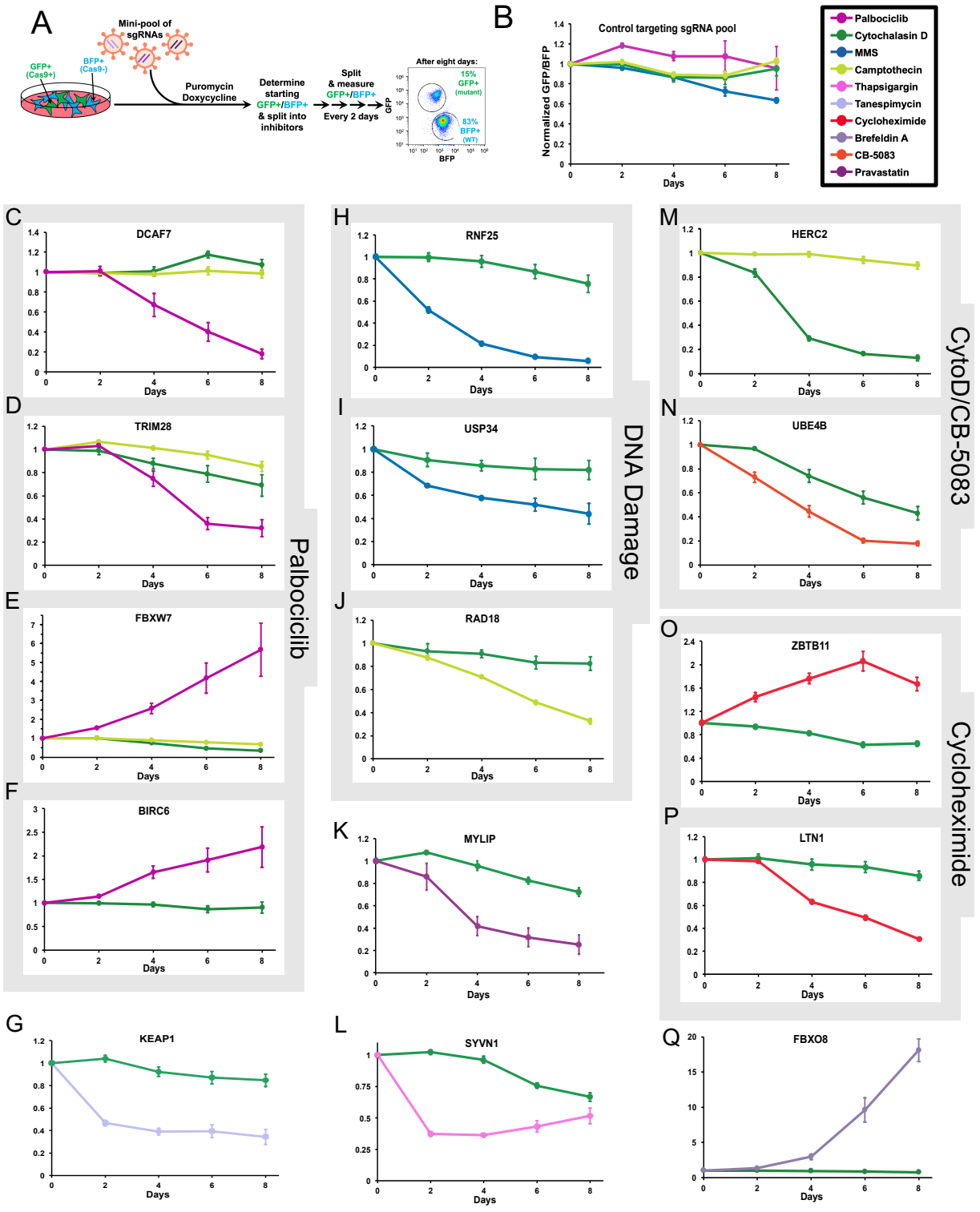


**Figure 1.5. Screen results validated using internally controlled, competitive growth assay.**
**(A)** Internally controlled, two color, competitive growth assay used to validate sensitive and resistant E3s and DUBs observed in the screen. Cas9$^{+}$ GFP$^{+}$ HAP1 cells were mixed with BFP-expressing WT HAP1 cells, infected with pools of 2-4 sgRNAs targeting one gene,

treated with puromycin and doxycycline to select for sgRNA integration and induce Cas9 expression, then split into media with or without one of several compounds every two days for eight days. The GFP/BFP ratio was measured by flow cytometry every two days.

**(B-Q)** Data represent the mean of four replicates ± SEM, first normalized to the day zero GFP/BFP ratios, and subsequently normalized to the untreated GFP/BFP ratio at each time point. [palbociclib]=1.5μM; [cytochalasin D]=60nM; [thapsigargin]= 8.08nM; [MMS]=9.75μg/mL; [camptothecin]= 1.0nM; [cycloheximide]= 340nM (targeting control), 256nM (LTN1); [tanespimycin]= 500nM (targeting control), 150nM (KEAP1); [pravastatin]=730μM; [brefeldin A]= 107nM; [CB-5083]=454nM

**(B)** Normalized GFP/BFP assay with targeting control sgRNAs (pool of 11) in palbociclib, cytochalasin D, MMS, and camptothecin.

**(C-Q)** Normalized GFP/BFP assays for 15 E3/DUB genes.

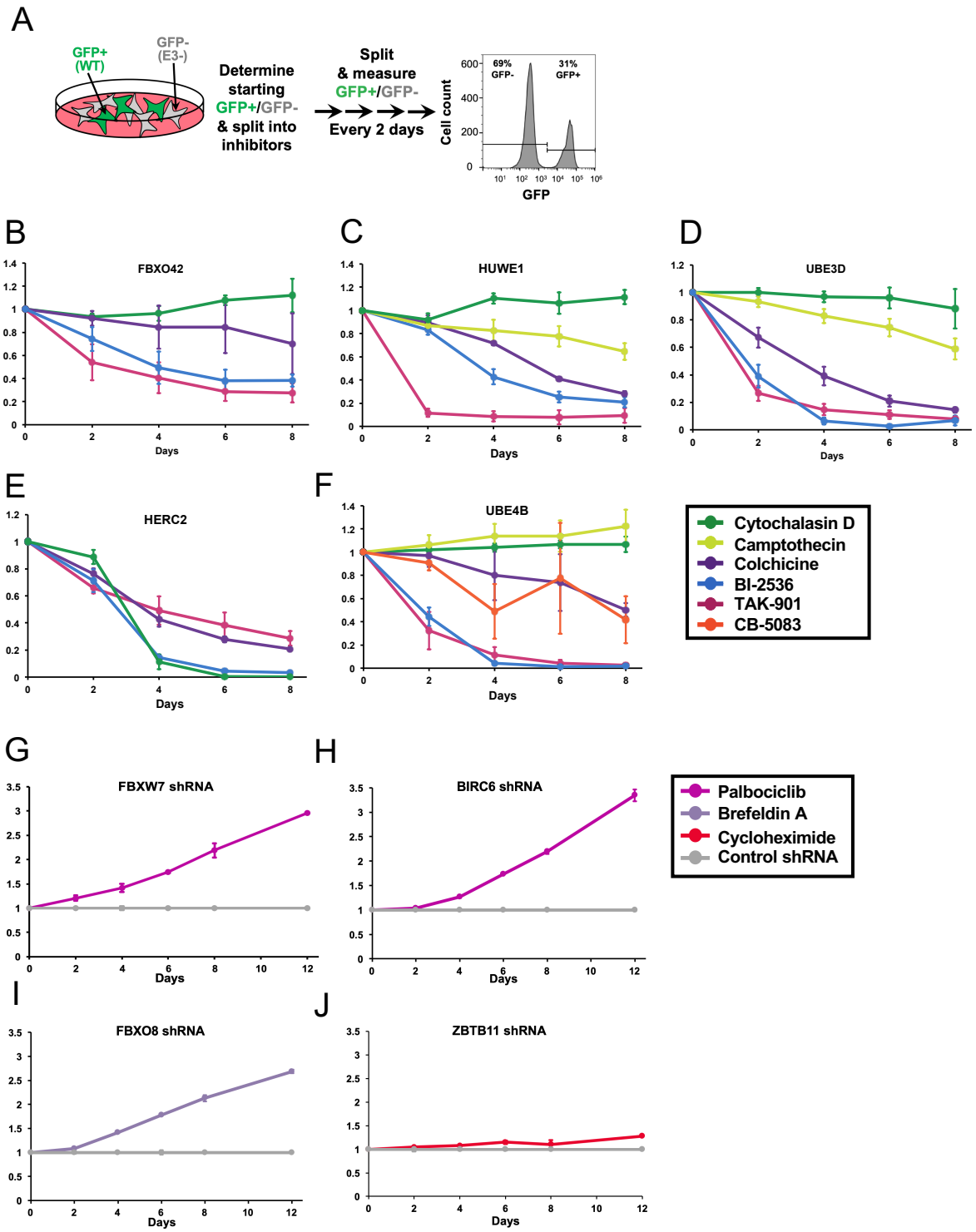


**Figure 1.6. FBXO42, HUWE1, UBE3D, HERC2, and UBE4B clonal mutant cell lines are highly sensitive to mitotic inhibitors.**

**(A)** Internally controlled, competitive growth assay with clonal E3 mutant HAP1 cells and WT GFP-expressing cells. After mixing, starting GFP+/– ratio was determined by flow cytometry, and mixes were split into media with or without one of several inhibitors every

two days for eight days (HAP1) or twelve days (U2OS). GFP+/– ratio was measured every two days by flow cytometry. Data were normalized to the day zero GFP+/– ratio, and subsequently normalized to the untreated GFP+/– ratio at each time point.

**(B)** Normalized GFP+/– assay for *FBXO42* mutant clone. Data represent the mean of three replicates ± SEM.

**(C)** Normalized GFP+/– assay for *HUWE1* mutant clones. Data represent the mean of five total replicates from two clones ± SEM.

**(D)** Normalized GFP+/– assay for *UBE3D* mutant clones. Data represent the mean of six total replicates from two clones ± SEM.

**(E)** Normalized GFP+/– assay for *HERC2* mutant clone. Data represent the mean of two replicates (BI-2536, colchicine, and TAK-901) to three replicates (cytochalasin D and untreated) from one clone ± SEM.

**(F)** Normalized GFP+/– assay for *UBE4B* mutant clone. Data represent the mean of two replicates (BI-2536 and colchicine) to three replicates (camptothecin, CB-5083, cytochalasin D, TAK-901, and untreated) from one clone ± SEM.

**(G)** Normalized GFP+/- assay for U2OS pool expressing shRNA against FBXW7 (TRCN0000355644), where data is first normalized to the day zero GFP+/- ratio, then to the untreated GFP+/- ratio at each time point, and subsequently normalized to the control shRNA. Data represent the mean of two replicates ± SEM.

**(H)** Normalized (as in G) GFP+/- assay for U2OS pool expressing shRNA against BIRC6 (TRCN0000364501). Data represent the mean of two replicates ± SEM.

**(I)** Normalized (as in G) GFP+/- assay for U2OS pool expressing shRNA against FBXO8 (TRCN0000034316). Data represent the mean of two replicates ± SEM.

**(J)** Normalized (as in G) GFP+/- assay for U2OS pool expressing shRNA against ZBTB11 (TRCN0000376563). Data represent the mean of two replicates ± SEM.

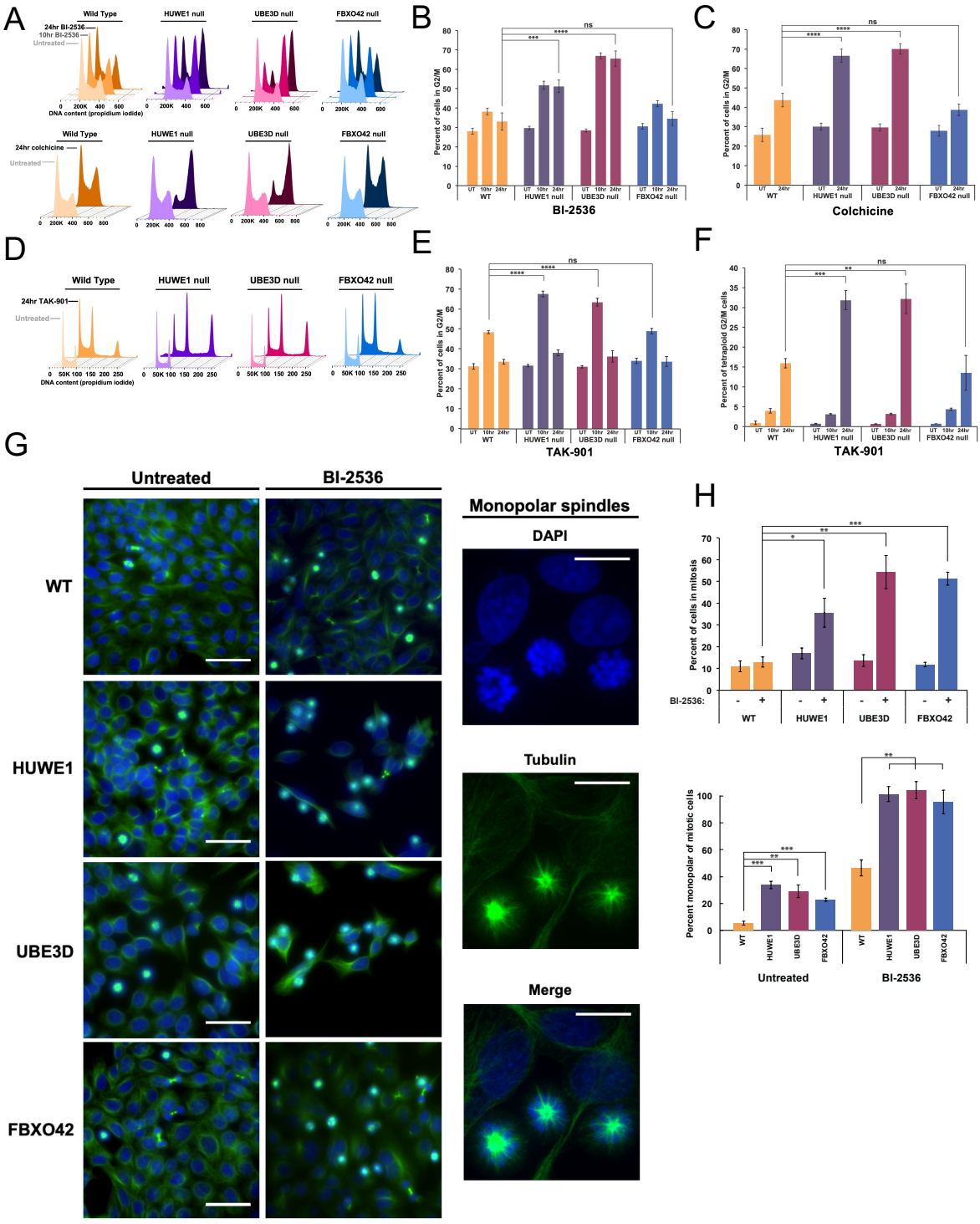


**Figure 1.7. FBXO42, HUWE1, and UBE3D are required for normal mitotic progression.**
**(A)** Representative propidium iodide-based cell cycle analysis by flow cytometry (with arbitrary units on the x-axis) of HAP1-Cas9 wild type cells and HAP1 clonal mutant cell lines of *FBXO42*, *HUWE1*, and *UBE3D* after 10h and 24h in 14.4nM BI-2536 and after 24h in 20nM colchicine. Untreated samples were collected at the 24h time point.

**(B)** Quantification of BI-2536 results in (A). Untreated (UT). Data represent the mean ± SEM, n=6-26.

**(C)** Quantification of colchicine results in (A). Data represent the mean ± SEM, n=5-12.

**(D)** Representative propidium iodide-based cell cycle analysis by flow cytometry (with arbitrary units on the x-axis) of HAP1-Cas9 wild type cells and HAP1 clonal mutant cell lines of *FBXO42*, *HUWE1*, and *UBE3D* after 10h and 24h in 200nM TAK-901. Untreated samples were collected at the 24h time point.

**(E)** Quantification of normal G2/M content in (D). Data represent the mean ± SEM, n=5-24.

**(F)** Quantification of polyploid G2/M content in (D). Data represent the mean ± SEM, n=5-24.

**(G)** Representative immunofluorescence images of HAP1-Cas9 wild type, *HUWE1*, *UBE3D* and *FBXO42* clonal mutant cell lines after 24h in 14.4nM BI-2536. Widefield images depicting untreated and treated (BI-2536) samples fixed at the 24h time point. Scale bars, 50 μm (left panel). Confocal images depicting example monopolar spindle morphologies after 24h of 14.4nM BI-2536 treatment. Scale bars, 15 μm (right panel). Green: microtubules; blue: DNA.

**(H)** **Top:** Quantification of the number of mitotic cells by IMF in HAP1-Cas9 wild type, *HUWE1*, *UBE3D* and *FBXO42* clonal mutant cell lines following 24h of 14.4nM BI-2536. **Bottom**: Quantification of the proportion of mitotic cells displaying monopolar spindles from the top panel. A minimum of 250 mitotic cells were counted per replicate. Data represent the mean ± SEM, n=3.

**(B-H)** (*) (**) (***) and (****) represent p-values of $\leq 0.05$, $\leq 0.01$, $\leq 0.001$, and $\leq 0.0001$, respectively.

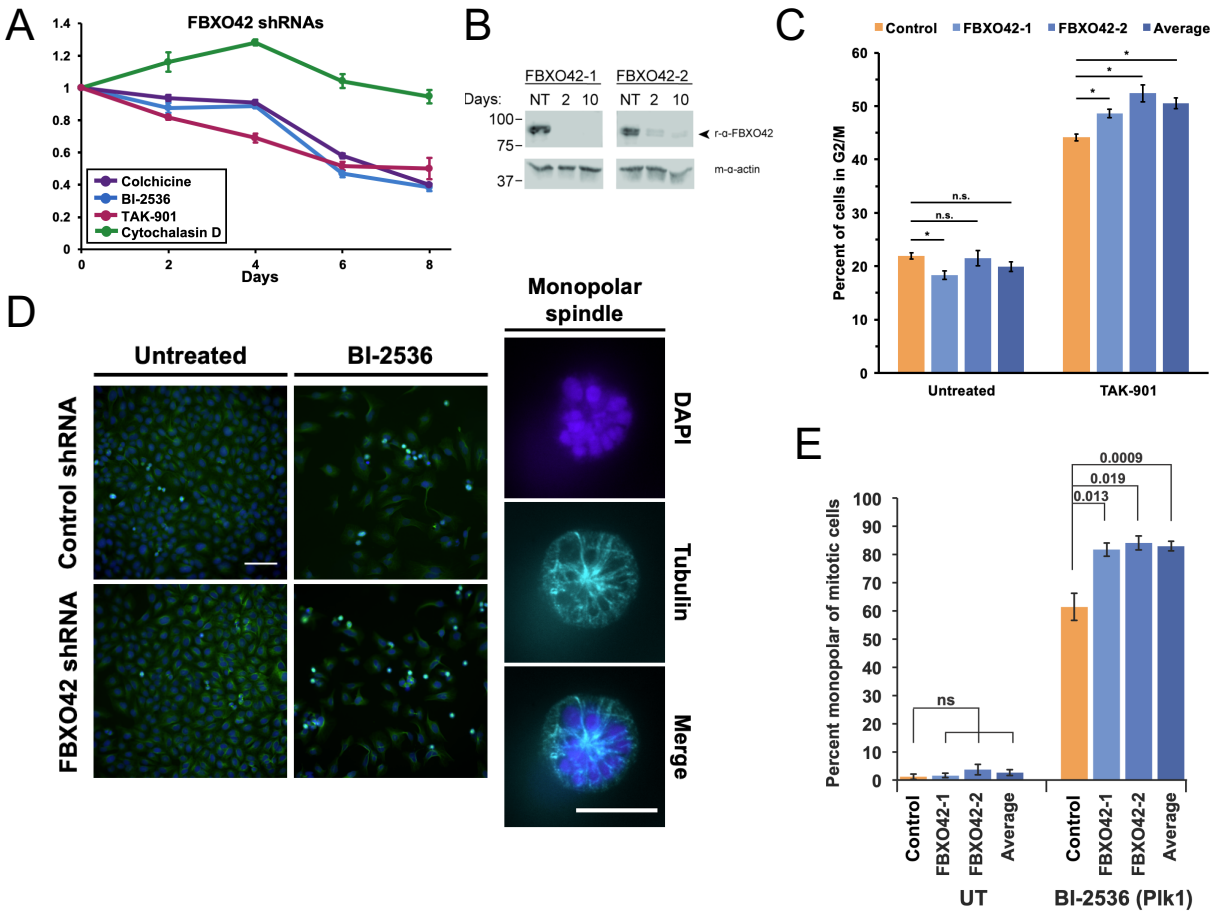


**Figure 1.8. FBXO42 plays a role in mitosis in osteosarcoma cell line U2OS.**

**(A)** Internally controlled, competitive growth assay. GFP$^+$ U2OS cells stably expressing a control shRNA (SHC002) were mixed with U2OS cells stably expressing one of two shRNAs against *FBXO42* (FBXO42-1: TRCN0000134822; FBXO42-2: TRCN00028599). The starting GFP+/– ratio was determined by flow cytometry, and cells were split into media with or without one of several inhibitors every two days for eight days, with flow cytometry analysis of the GFP+/– ratio every two days. In parallel, GFP$^+$ U2OS stably expressing SHC002 were mixed with GFP$^-$ U2OS stably expressing SHC002. Data were normalized to the day zero GFP+/– ratio, subsequently normalized to the untreated GFP+/– ratio at each time point, and finally normalized to the GFP$^+$ SHC002/GFP$^-$ SHC002 data. Data represent the mean of six replicates (three of each FBXO42 shRNA) ± SEM. [BI-2536]=24nM; [TAK-901]=19.8-24.8nM; [colchicine]=9.39nM; [cytochalasin D]=39.4nM. All cells were grown in 2µg/mL puromycin for the duration of the experiment to maintain selection for the integrated shRNAs.

**(B)** Western blots of samples from (A) stably expressing shRNAs against *FBXO42* collected at days 2 and 10, or cells expressing the control shRNA SHC002 (NT) (ABclonal antibody). FBXO42-1 and FBXO42-2 as in (A).

**(C)** Quantification of propidium iodide-based cell cycle analysis by flow cytometry of U2OS cells stably expressing shRNAs against *FBXO42* or control shRNA and treated with 609nM TAK-901 for 24h. Data represent the mean of 6 replicates ± SEM for FBXO42-1 and

FBXO42-2, and 12 replicates ± SEM for Control and Average (the average of FBXO42-1 and FBXO42-2). Control is the average of Control-1 (U2OS-WT with SHC002) and Control-2 ($GFP^+$ cells with SHC002). (*) indicates p-value ≤ 0.005.

**(D)** Representative widefield immunofluorescence images of U2OS cells expressing a control shRNA (SHC002) or FBXO42 shRNA after 24h in 24nM BI-2536 or untreated. Scale bar=100 μm (left panel). Confocal images depicting example monopolar spindle morphology after 24h of 24nM BI-2536 treatment. Scale bar=15 μm (right panel). Green: microtubules; blue: DNA.

**(E)** Quantification of the proportion of mitotic cells displaying monopolar spindles in U2OS cells stably expressing a control shRNA (WT) or one of two shRNAs against *FBXO42* and treated with 24nM BI-2536 for 24h. FBXO42-1, FBXO42-2 and Control as described in (A). A minimum of 250 mitotic cells were counted per replicate. Data represent the mean ± SEM, n=3.

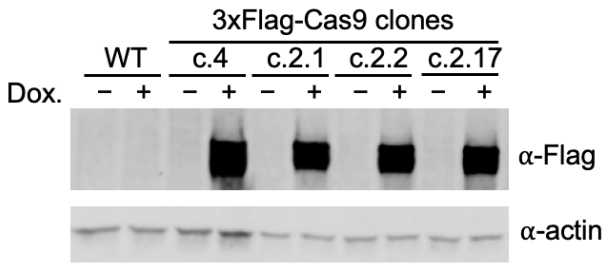


**Figure 1.S1.** Western blot of four independent HAP1-Cas9 clones containing doxycycline-inducible 3xFlag-Cas9. To induce Cas9, cells were given fresh media with 1µg/mL doxycycline every day for three days, then collected at day 4 for WB. The CRISPR-Cas9 screens were done in triplicate using three of these four clones (either c.2.1, c.2.2, and c.2.17 or c.2.1, c.2.2, and c.4).

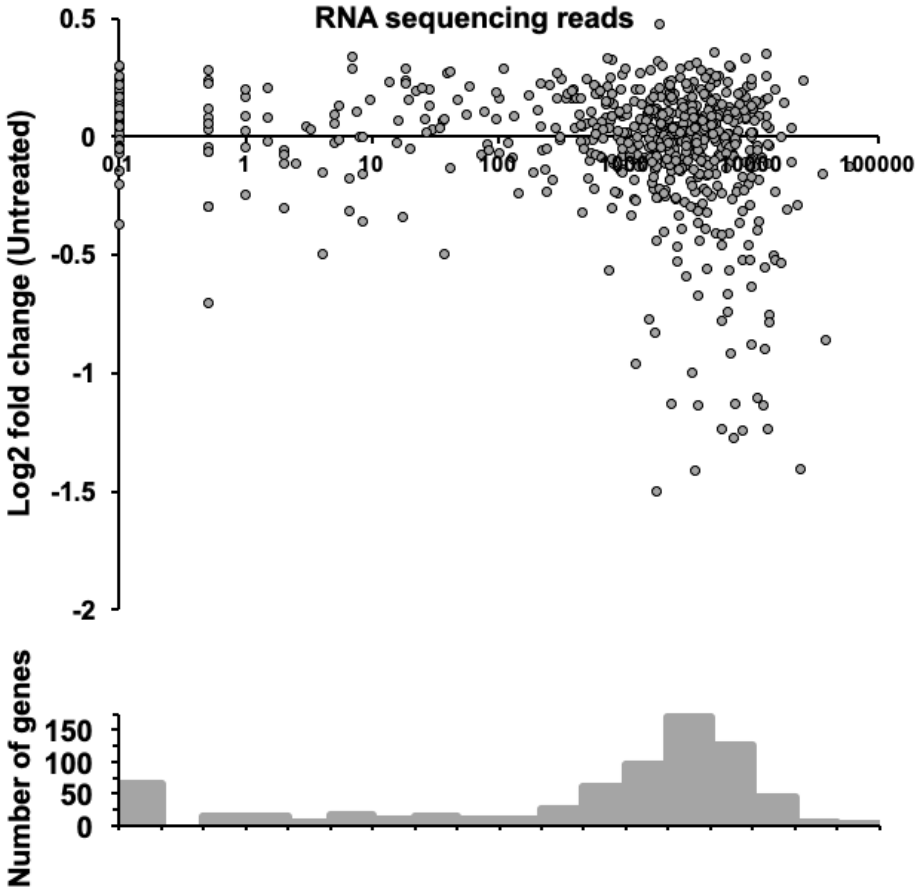


**Figure 1.S2.** Correlation between the untreated gene Log2 fold change scores (from the median of 15 replicates) and gene expression. RNA sequencing data are the average of two replicates of WT HAP1 cells, raw sequencing reads (Lumb et al., 2017). For the purposes of this plot, genes with no detected sequencing reads were set to 0.1. **Bottom:** Histogram of the number of genes in each RNA sequencing read bin.

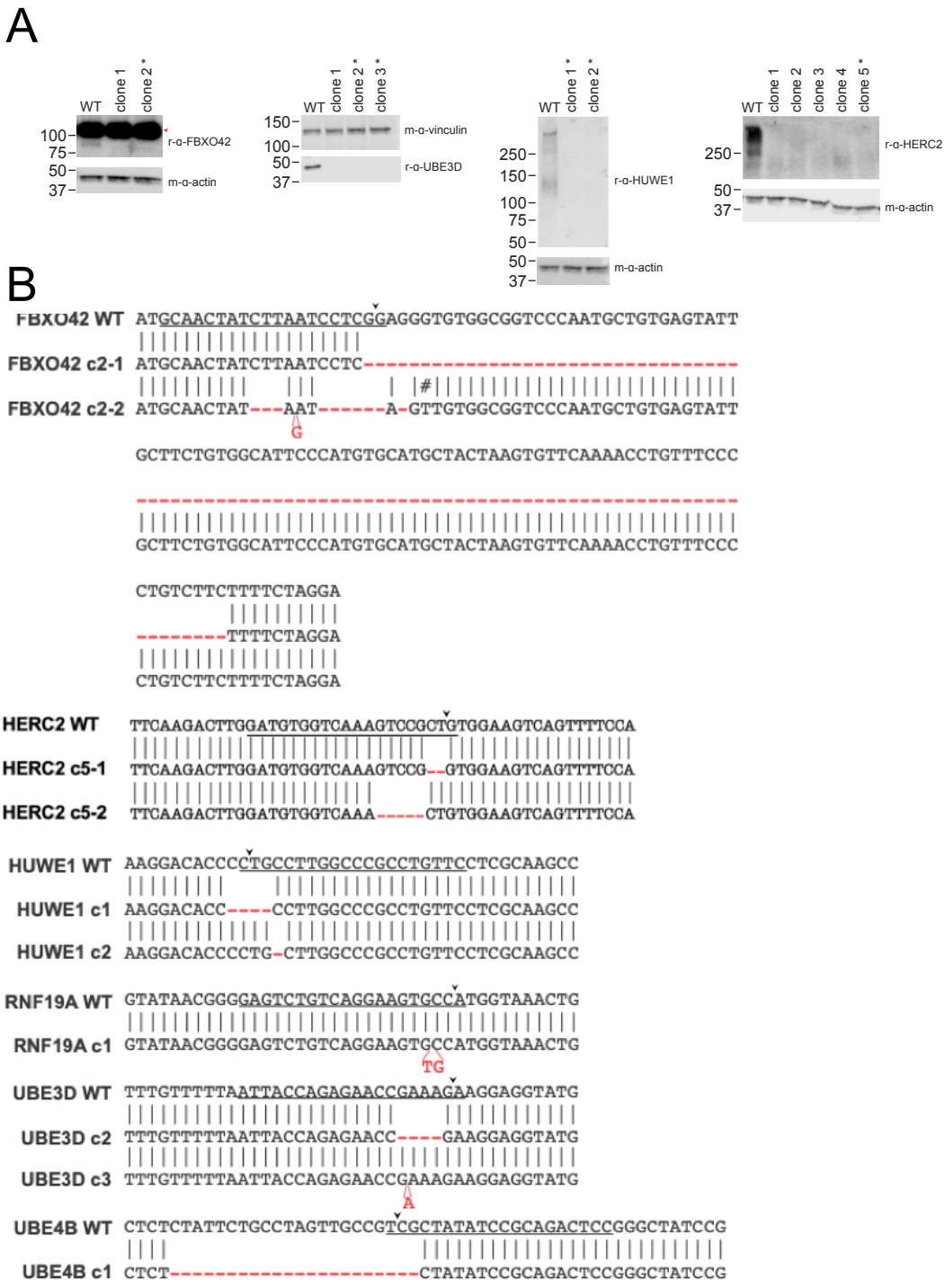


**Figure 1.S3.**

**(A)** Western blots of *FBXO42*, *UBE3D*, HUWE1, and *HERC2* mutant clones. Large non-specific band in the FBXO42 blot is indicated by a red arrow (Aviva Systems Bio FBXO42 antibody). Clones used in this study are indicated by asterisks.

**(B)** Sanger sequencing results of the sgRNA region of each target gene. Regions were PCR amplified from genomic DNA and PCR products were purified before being subjected to

Sanger sequencing. The wild type sequence for each gene is shown on top, and the clonal mutant sequences are shown below. Predicted Cas9 cut sites are indicated by black arrows, the sequence complementary to the sgRNA is underlined in black, deletions are indicated by dashed red lines, and insertions are indicated by red bases. For FBXO42 and HERC2, each allele had a different edit (denoted by c2-1 and c2-2 or c5-1 and c5-2, respectively).

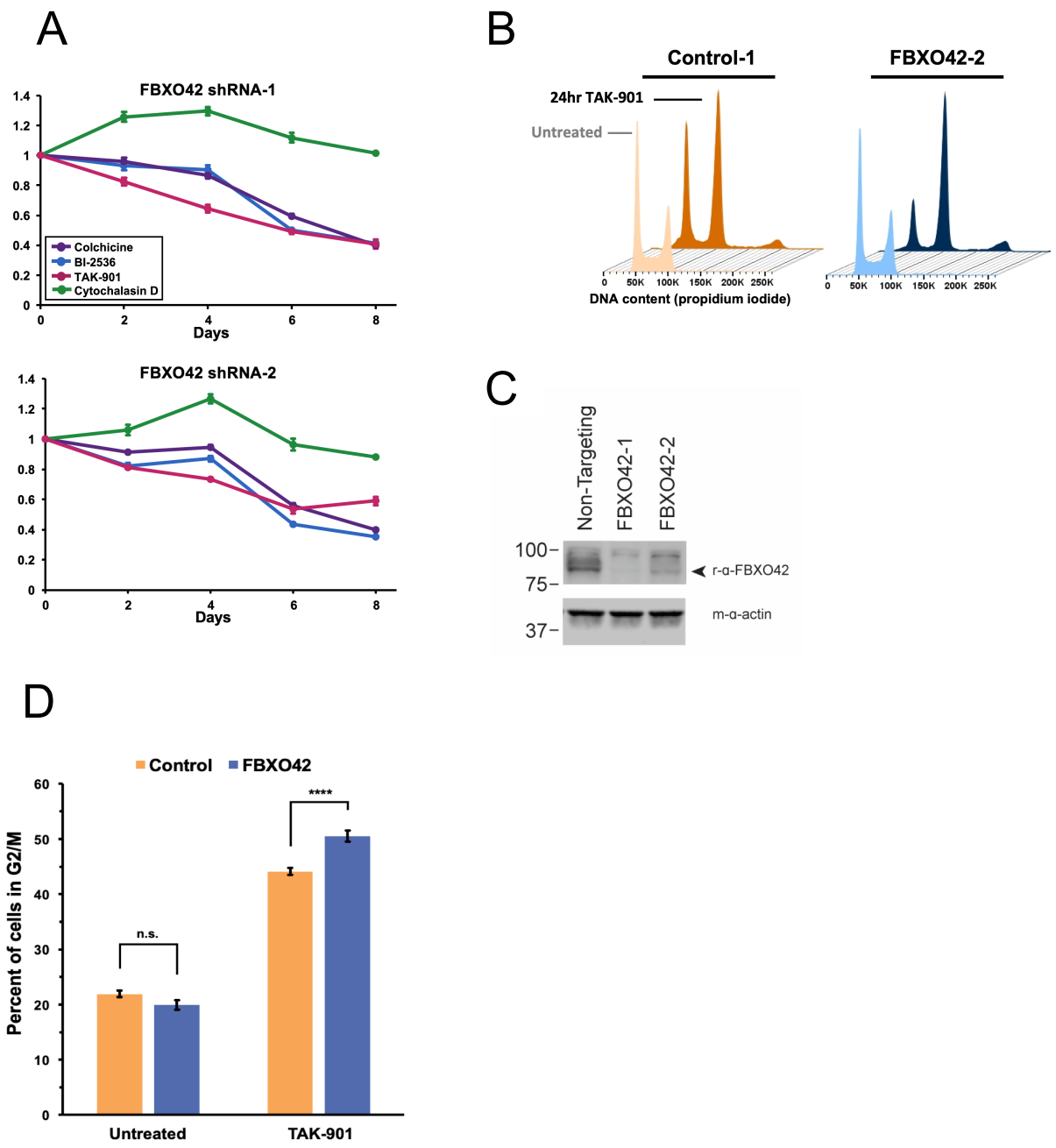


**Figure 1.S4.**

**(A)** Internally controlled, competitive growth assays from Figure 1.8A showing the two shRNAs against FBXO42 separately. Data represent the mean of three replicates for each FBXO42 shRNA ± SEM. FBXO42-1 and FBXO42-2 as in Figure 1.8A.

**(B)** Representative propidium iodide-based cell cycle analysis (with arbitrary units on the x-axis) of U2OS cells stably expressing shRNAs against *FBXO42* or control shRNA treated with 609nM TAK-901 for 24 hours (quantification in Figure 1.8C). Untreated samples were collected at the 24hr time point. FBXO42-2: TRCN00028599; Control-1: U2OS WT cells with SHC002.

**(C)** Western blot of U2OS cells stably expressing shRNAs against *FBXO42* or control shRNA (ABclonal antibody). Samples are from the same experiment as (Figure 1.8C). FBXO42-1: TRCN0000134822; FBXO42-2: TRCN00028599; Control/Non-targeting: SHC002.

**(D)** U2OS propidium iodide-based cell cycle analysis quantification from Figure 1.8C showing just the average of two shRNAs against FBXO42 and the average of Control-1 and Control-2. Data represent the mean of 12 replicates ± SEM (****) indicates p-value ≤ 0.0001. Untreated samples were collected at the 24h time point.

A

| | CUL4A/4B are: | |
|---|---|---|
| | Resistant to TTFA | Sensitive to BI-2536 |
| SRs: | DCAF11 0.60 | |
| | DCAF5 0.46 | |

B

| | CUL3 is: | | | | | |
|---|---|---|---|---|---|---|
| | Sensitive to Flavo | | Sensitive to Tanespimycin | | Resistant to BI-2536 | |
| SRs: | ZBTB7A | -0.50 | KEAP1 | -1.50 | NACC1 | 0.63 |

C

| | CUL2 is: | | | | CUL5 is: | | | | | | | | | |
|---|---|---|---|---|---|---|---|---|---|---|---|---|---|---|
| | Resistant to Pimasertib | | Resistant to TTFA | | Sensitive to TTFA | | Sensitive to Leptomycin | | Resistant to Palbociclib | | Resistant to Ribociclib | | Resistant to Pictilisib | |
| SRs: | | | SOCS4 | 0.86 | SOCS4 | 0.86 | WSB2 | -0.71 | | | | | | |
| | | | TCEB3 | 0.71 | TCEB3 | 0.71 | | | | | | | | |

**Figure 1.S5. Specific cullin RING ligase substrate receptors (SRs) often correlate with data seen for their associated cullins.** Data for cullins and their SRs with strong Log2 fold change scores (≤-0.45 or ≥0.45) and p-values ≤0.01 are shown. Since CUL4A and CUL4B are likely redundant, a Log2 fold change cut-off of ≤-0.20 or ≥0.20 for both of these cullins was used.

**(A)** CUL4A and CUL4B both showed modest resistance to TTFA ($\bar{x}$ = 0.25) and modest sensitivity to BI-2536 ($\bar{x}$ = -0.34). DCAF11 and DCAF5 mutants were significantly resistant to TTFA, whereas no single SR showed strong sensitivity to BI-2536, suggesting a combinatorial effect.

**(B)** CUL3 was significantly sensitive to flavopiridol and tanespimycin, and resistant to BI-2536. In each case, one CUL3 SR showed a similarly strong response.

**(C)** CUL2 and CUL5, which share SRs, were significantly sensitive or resistant to pimasertib, TTFA, leptomycin B, palbociclib, ribociclib, and pictilisib. The SR SOCS4 and adapter TCEB3 likely explain the TTFA resistance of CUL2, whereas WSB2 appears responsible for the sensitivity of CUL5 to leptomycin B. No single SR showed a significant response to pimasertib, palbociclib, ribociclib, or pictilisib, suggesting a strong combinatorial effect.

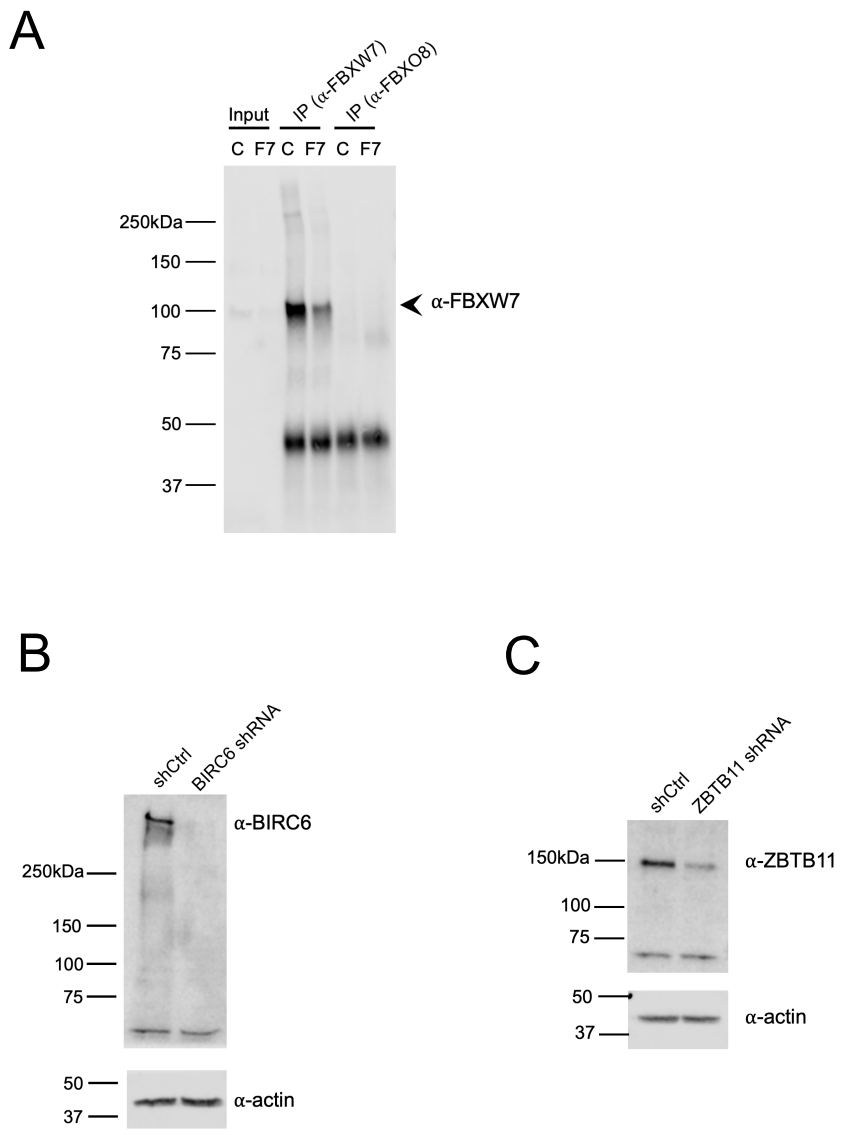


**Figure 1.S6.**

**(A)** Immunoprecipitation of FBXW7 from U2OS cells expressing a non-targeting control shRNA (C) or an shRNA against FBXW7 (F7). IP performed with FBXW7 antibody A301-721A or FBXO8 antibody (IgG control) ab228838, and Western blot probed with FBXW7 antibody A301-720A. Loading was 1x input and 200x IP. FBXW7 shRNA: TRCN0000355644.

**(B)** Western blot of U2OS cells expressing a non-targeting control shRNA (shCtrl) or an shRNA targeting BIRC6 (TRCN0000364501). Samples collected concurrently to experiment in Figure 1.6H.

**(C)** Western blot of U2OS cells expressing a non-targeting control shRNA (shCtrl) or an shRNA against ZBTB11 (TRCN0000376563). Samples collected concurrently to experiment in Figure 1.6J.

BI-2536

| | Sensitive | | Resistant | |
|---|---|---|---|---|
| | Gene | FDR | Gene | FDR |
| 1 | UBE4B | 0.000159 | SMURF1 | 0.000184 |
| 2 | FBXW7 | 0.000159 | MIB1 | 0.000184 |
| 3 | RNF146 | 0.000159 | CNOT4 | 0.000184 |
| 4 | FBXO42 | 0.000159 | SKP2 | 0.000184 |
| 5 | PCGF3 | 0.000159 | RNF11 | 0.000184 |
| 6 | RNF19A | 0.000159 | FBXW11 | 0.000184 |
| 7 | RNF19B | 0.000159 | NACC1 | 0.000184 |
| 8 | STUB1 | 0.000159 | OTUD6B | 0.000184 |
| 9 | WDTC1 | 0.000159 | PHIP | 0.000184 |
| 10 | UBR5 | 0.000159 | FBXO11 | 0.000184 |
| 11 | IVNS1ABP | 0.000159 | MKRN1 | 0.000184 |
| 12 | HERC2 | 0.000159 | NEURL1B | 0.000184 |
| 13 | CUL4A | 0.000159 | PJA1 | 0.000184 |
| 14 | KDM2B | 0.000159 | KLHL20 | 0.000184 |
| 15 | HUWE1 | 0.000159 | MNAT1 | 0.000184 |
| 16 | PCGF5 | 0.000159 | ZBTB24 | 0.000184 |
| 17 | LRRC41 | 0.000159 | TRIM24 | 0.000184 |
| 18 | ZBTB1 | 0.000159 | ASB10 | 0.000184 |
| 19 | ZRANB1 | 0.000159 | ASB3 | 0.000184 |
| 20 | ZBTB10 | 0.000159 | USP7 | 0.000456 |
| 21 | ZBTB14 | 0.000159 | ZNRF1 | 0.000456 |
| 22 | FBXL11 | 0.000159 | KLHL13 | 0.000456 |
| 23 | PPIL2 | 0.000456 | ANKIB1 | 0.000456 |
| 24 | CBLL1 | 0.000564 | PEX12 | 0.000672 |
| 25 | BRCA1 | 0.000564 | RNF145 | 0.000672 |
| 26 | UBR7 | 0.000564 | RNF148 | 0.000672 |
| 27 | TRIM28 | 0.000564 | CUL3 | 0.001124 |
| 28 | NOSIP | 0.000564 | CUL1 | 0.001124 |
| 29 | ZBTB2 | 0.000564 | TRIM38 | 0.007576 |
| 30 | BARD1 | 0.000564 | MDM4 | 0.007355 |
| 31 | KEAP1 | 0.000564 | SMURF2 | 0.010038 |
| 32 | RNF220 | 0.00068 | KBTBD8 | 0.012088 |
| 33 | RNF214 | 0.00068 | MSL2 | 0.012088 |
| 34 | DCAF15 | 0.001564 | RNF14 | 0.012088 |
| 35 | TCEB1 | 0.00068 | BTBD7 | 0.012088 |
| 36 | SPOP | 0.00068 | PCGF6 | 0.028263 |
| 37 | USP46 | 0.00068 | FBXO38 | 0.041689 |
| 38 | PRPF19 | 0.000851 | BIRC6 | 0.041689 |
| 39 | UBE3D | 0.002303 | ITCH | 0.041689 |
| 40 | RNF219 | 0.002303 | FBXL13 | 0.069686 |
| 41 | TRIM48 | 0.002303 | FBXO4 | 0.069686 |
| 42 | OTUD7B | 0.002356 | | |
| 43 | BAP1 | 0.002356 | | |
| 44 | TRAF2 | 0.002356 | | |
| 45 | KLHL28 | 0.002356 | | |
| 46 | TRIM35 | 0.002356 | | |
| 47 | TRIM49A | 0.005172 | | |
| 48 | TRIM49C | 0.005172 | | |
| 49 | FBXO28 | 0.005209 | | |
| 50 | TCEB2 | 0.005828 | | |
| 51 | FEM1A | 0.005828 | | |
| 52 | ZNF598 | 0.007692 | | |
| 53 | TRAF4 | 0.007692 | | |
| 54 | UBR4 | 0.007692 | | |
| 55 | ZBTB4 | 0.007692 | | |
| 56 | VHL | 0.009826 | | |
| 57 | MARCH4 | 0.009826 | | |
| 58 | HECTD1 | 0.009826 | | |
| 59 | TRIM59 | 0.010608 | | |
| 60 | RNF113A | 0.012762 | | |
| 61 | TRIML1 | 0.014685 | | |
| 62 | CBL | 0.014685 | | |
| 63 | USP31 | 0.014685 | | |
| 64 | RNF207 | 0.014685 | | |
| 65 | ZBTB7A | 0.014685 | | |
| 66 | TRAIP | 0.023327 | | |
| 67 | RNF2 | 0.018913 | | |
| 68 | RNF43 | 0.02559 | | |
| 69 | RCBTB1 | 0.02559 | | |
| 70 | MGRN1 | 0.027622 | | |
| 71 | RNF215 | 0.030258 | | |
| 72 | KLHL26 | 0.030258 | | |
| 73 | KLHL18 | 0.030258 | | |
| 74 | ZBTB17 | 0.030258 | | |
| 75 | RNFT1 | 0.030258 | | |
| 76 | FBXO5 | 0.030258 | | |
| 77 | DCAF11 | 0.030258 | | |
| 78 | BIRC8 | 0.030258 | | |
| 79 | FBXO2 | 0.03632 | | |
| 80 | RNF224 | 0.03632 | | |
| 81 | HECTD3 | 0.040168 | | |
| 82 | CGRRF1 | 0.040168 | | |
| 83 | CUL4B | 0.040168 | | |
| 84 | FBXO34 | 0.040168 | | |
| 85 | HIC1 | 0.048416 | | |
| 86 | ANKFY1 | 0.053783 | | |
| 87 | TRIM46 | 0.053783 | | |
| 88 | PDZRN3 | 0.053783 | | |
| 89 | ZBTB40 | 0.053783 | | |
| 90 | FBXW5 | 0.058034 | | |
| 91 | RBBP6 | 0.058034 | | |
| 92 | ASB5 | 0.058034 | | |
| 93 | TRIM33 | 0.062387 | | |
| 94 | ANAPC11 | 0.062387 | | |
| 95 | DCAF4L2 | 0.062387 | | |
| 96 | KBTBD7 | 0.062387 | | |
| 97 | TRIM9 | 0.062387 | | |
| 98 | SOCS1 | 0.062387 | | |
| 99 | LONRF1 | 0.062387 | | |
| 100 | FBXO43 | 0.062387 | | |
| 101 | KLHL40 | 0.062387 | | |
| 102 | AMBRA1 | 0.062387 | | |
| 103 | CHFR | 0.062387 | | |
| 104 | FBXL6 | 0.062387 | | |
| 105 | UCHL3 | 0.062387 | | |
| 106 | BTBD16 | 0.062387 | | |
| 107 | RFPL1 | 0.062387 | | |
| 108 | MARCH7 | 0.062387 | | |
| 109 | SYVN1 | 0.069064 | | |
| 110 | CCIN | 0.071173 | | |
| 111 | RFPL2 | 0.071173 | | |
| 112 | ZBTB48 | 0.071173 | | |
| 113 | FBXO3 | 0.071173 | | |
| 114 | DCAF13 | 0.071173 | | |
| 115 | SIAH3 | 0.071173 | | |
| 116 | FBXO48 | 0.071173 | | |
| 117 | G2E3 | 0.071173 | | |
| 118 | KLHL36 | 0.080735 | | |
| 119 | ASB2 | 0.071173 | | |
| 120 | MARCH8 | 0.071173 | | |
| 121 | UBE4A | 0.071173 | | |
| 122 | TRIM36 | 0.071173 | | |
| 123 | RBX1 | 0.088533 | | |
| 124 | TRIM52 | 0.088533 | | |
| 125 | KLHL1 | 0.088533 | | |
| 126 | UBR3 | 0.088533 | | |
| 127 | KLHL22 | 0.088533 | | |
| 128 | FBXW10 | 0.088533 | | |
| 129 | TRIM65 | 0.091641 | | |
| 130 | ARIL1 | 0.094809 | | |
| 131 | DCAF6 | 0.110847 | | |

Palbociclib

| | Sensitive | | Resistant | |
|---|---|---|---|---|
| | Gene | FDR | Gene | FDR |
| 1 | DCAF7 | 0.000437 | FBXW7 | 7.40E-05 |
| 2 | ARMC5 | 0.000437 | FBXL5 | 7.40E-05 |
| 3 | TRIM28 | 0.000437 | BIRC6 | 7.40E-05 |
| 4 | STUB1 | 0.000437 | NOSIP | 7.40E-05 |
| 5 | FBXO11 | 0.000437 | FBXO33 | 7.40E-05 |
| 6 | SKP2 | 0.000437 | RNF7 | 7.40E-05 |
| 7 | UBE4B | 0.000437 | RFWD2 | 7.40E-05 |
| 8 | USP1 | 0.001943 | ARIH2 | 7.40E-05 |
| 9 | PJA1 | 0.002448 | CUL5 | 7.40E-05 |
| 10 | RNF219 | 0.013668 | UBR4 | 7.40E-05 |
| 11 | UBE3C | 0.022324 | LZTR1 | 7.40E-05 |
| 12 | FBXO28 | 0.022324 | VPS18 | 7.40E-05 |
| 13 | KBTBD2 | 0.023726 | TRIM64B | 7.40E-05 |
| 14 | ZBTB14 | 0.02571 | CNOT4 | 7.40E-05 |
| 15 | FBXO45 | 0.02571 | IRF2BP1 | 7.40E-05 |
| 16 | MARCH6 | 0.02571 | CISH | 7.40E-05 |
| 17 | TCEB3 | 0.033741 | UHRF1 | 7.40E-05 |
| 18 | VHL | 0.033741 | MYLIP | 7.40E-05 |
| 19 | CUL4B | 0.033741 | SIAH1 | 7.40E-05 |
| 20 | FBXL14 | 0.104761 | RNF214 | 7.40E-05 |
| | | | OTUD7A | 7.40E-05 |
| | | | PCGF6 | 7.40E-05 |
| | | | CBL | 7.40E-05 |
| | | | VPS11 | 7.40E-05 |
| | | | RNF2 | 7.40E-05 |
| | | | FBXO36 | 7.40E-05 |
| | | | RNF138 | 7.40E-05 |
| | | | ZBTB44 | 7.40E-05 |
| | | | ASB13 | 7.40E-05 |
| | | | KBTBD13 | 7.40E-05 |
| | | | RNF126 | 7.40E-05 |
| | | | TRAF7 | 7.40E-05 |

**Figure 1.S7. Comparison of primary analysis with FDR analysis for BI-2536 and palbociclib.**
Genes are ranked by FDR analysis for sensitivity or resistance to BI-2536 or palbociclib. FDR scores of genes identified as sensitive are indicted in dark red if they have an FDR< 0.05 and light red if 0.05<FDR<0.1. FDR scores of genes whose loss causes resistance are shown in dark blue if they have and FDR < 0.05 and light blue if 0.05<FDR<0.1. All genes identified as having significant sensitivity or resistance to BI-2536 or palbociclib in our primary analysis are included and are highlighted in yellow. Not all genes with significant FDRs are indicated, as this test was considerably less stringent. The complete FDR list can be found in the peer-reviewed publication.

**Table 1.S1. Key Resources Table**

| Antibodies | | |
|---|---|---|
| **Reagent or Resource** | **Source** | **Identifier** |
| Monoclonal anti-β-Actin antibody | Sigma | Cat#A5441; RRID AB_476744 |
| Monoclonal anti-Vinculin antibody | Sigma | Cat#V9131; RRID AB_477629 |
| Monoclonal anti-FLAG M2 antibody | Sigma | Cat#F3165; RRID AB_259529 |
| Polyclonal anti-UBE3D antibody | abcam | Cat#ab121927; RRID AB_11129761 |
| Polyclonal anti-FBXO42 antibody | ABclonal | Cat#A14898; RRID AB_2761778 |
| Polyclonal anti-FBXO42 antibody | Aviva Systems Bio | Cat#ARP47068_P050; RRID AB_2045869 |
| Polyclonal anti-HUWE1 antibody | Simon Wing lab | N/A |
| Polyclonal anti-FBXW7 antibody | Bethyl Laboratories | Cat#A301-720A; RRID AB_1210897 |
| Polyclonal anti-FBXW7 antibody | Bethyl Laboratories | Cat#A301-721A; RRID AB_1210898 |
| Monoclonal anti-BIRC6 antibody | Cell Signaling Technology | Cat#8756S; RRID AB_11220435 |
| Polyclonal anti-ZBTB11 antibody | Bethyl Laboratories | Cat#303-239A; RRID AB_10953662 |
| Dynabeads Protein A for immunoprecipitation | ThermoFisher | Cat#10001D |
| Goat Anti-rabbit IgG (H+L)-HRP conjugate | Bio-Rad | Cat#1721019; RRID AB_11125143 |
| Goat Anti-mouse IgG (H+L)-HRP conjugate | Bio-Rad | Cat#1721011; RRID AB_11125936 |
| Goat Anti-mouse IgG IRDye 800CW | LI-COR | Cat#92632210; RRID AB_621842 |
| Protein A-HRP conjugate | Bio-Rad | Cat#1706522 |
| Polyclonal Anti-tubulin Alexa Fluor 488 conjugate | Cell Signaling Technology | Cat#8058S; RRID AB_10860077 |

| **Bacterial and Virus Strains** | | |
|---|---|---|
| **Reagent or Resource** | **Source** | **Identifier** |
| DH5α subcloning competent cells | This study | N/A |
| XL-10 Gold Ultracompetent Cells | Agilent Technologies | Cat#200315 |
| MegaX DH10B T1R Electrocomp cells | ThermoFisher | Cat#C640003 |
| **Chemicals, Peptides, and Recombinant Proteins** | | |
| Complete EDTA free protease inhibitor cocktail | Roche | Cat#05056489001 |
| Leupeptin | Sigma | Cat#L2023 |
| Bestatin | Sigma | Cat#B8385 |
| Benzamidine HCl | Sigma | Cat#B6506 |
| 17-AAG/Tanespimycin | Cayman | Cat#75747-14-7 |
| BAPTA-AM | Cayman | Cat#126150-97-8 |
| BI-2536 | Cayman | Cat#755038-02-9 |
| Bleocin | EMD Millipore Calbiochem | Cat#203408 |
| Bortezomib | EMD Millipore Calbiochem | Cat#179324-69-7 |
| Brefeldin A | Cayman | Cat#20350-15-6 |
| Camptothecin | Sigma | Cat#C9911 |
| CB-5083 | Cayman | Cat#1542707-92-9 |
| Cisplatin | Sigma | Cat#479306 |
| Colchicine | Sigma | Cat#6-96-8 |

| Chemicals, Peptides, and Recombinant Proteins | | |
|---|---|---|
| **Reagent or Resource** | **Source** | **Identifier** |
| Cycloheximide | Sigma | Cat#C4859 |
| Cytochalasin D | Sigma | Cat#22144-77-0 |
| 2-[2-[4-(trifluoromethoxy)phenyl]hydrazinylidene]-propanedinitrile (FCCP) | Cayman | Cat#370-86-5 |
| Flavopiridol | Enzo Life Science | Cat#146426-40-6 |
| Bisindolylm. (bisindolylmaleimide/GF109203X) | Apexbio | Cat#133052-90-1 |
| Harringtonine | Abcam | Cat#26833-85-2 |
| Imatinib mesylate | Cayman | Cat#220127-57-1 |
| Ionomycin | AdipoGen Life Sciences | Cat#56092-81-0 |
| Ionomycin | Cayman | Cat#56092-81-0 |
| Ipatasertib (GDC-0068) | Cayman | Cat#1001264-89-6 |
| JG-231 | Laboratory of Jason Gestiwicki, UCSF | N/A |
| Latrunculin A | Enzo Life Science | Cat#76343-93-6 |
| Leptomycin B | Cayman | Cat#87081-35-4 |
| Methyl methanesulfonate (MMS) | ThermoFisher | Cat#66-27-3 |
| Nicotinamide | Cayman | Cat#98-92-0 |
| Paclitaxel (Taxol) | Cayman | Cat#33069-62-4 |
| Palbociclib/PD 0332991 isethionate | Sigma | Cat#827022-33-3 |

| Chemicals, Peptides, and Recombinant Proteins | | |
|---|---|---|
| **Reagent or Resource** | **Source** | **Identifier** |
| Pictilisib (GDC-0941) | Cayman | Cat#957054-30-7 |
| Pimasertib (AS-703026) | Cayman | Cat#1236699-92-5 |
| Pladienolide B | EMD Millipore Calbiochem | Cat#445493-23-2 |
| Pravastatin Sodium salt | Abcam | Cat#81131-70-6 |
| Rapamycin | Sigma | Cat#53123-88-9 |
| Ribociclib (Lee011) | Cayman | Cat#1211441-98-3 |
| RO-3306 | Cayman | Cat#872573-93-8 |
| SAHA/Vorinostat | Cayman | Cat#149647-78-9 |
| Dichloroacetic acid | Acros organics | Cat#2156-56-1 |
| TAK-901 | Apexbio | Cat#934541-31-8 |
| Thapsigargin | Sigma | Cat#67526-95-8 |
| Thenoyltrifluoroacetone (TTFA) | MP Biomedicals | Cat#326-91-0 |
| Tunicamycin | EMD Millipore Calbiochem | Cat#11089-65-9 |
| Vinblastine sulfate salt | Sigma | Cat#143-67-9 |
| Vectashield Anti-fade Mounting Medium | Fisher Scientific | Cat#NC9265087 |
| **Critical Commercial Assays** | | |
| Ex Taq DNA Polymerase | Takara Bio | Cat#RR001B |
| pGEM T-Easy Vector System | Promega | Cat#A1360 |
| MycoAlert Mycoplasma Detection Kit | Lonza | Cat# LT07-118 |

| **Critical Commercial Assays** | | |
|---|---|---|
| **Reagent or Resource** | **Source** | **Identifier** |
| Pierce BCA Protein Assay Kit | ThermoFisher | Cat# 23225 |
| QIAprep Spin Miniprep kit | Qiagen | Cat# 27106 |
| Nucleospin Blood L kit | Machery Nagel | Cat# 740954.20 |
| Lenti-X concentrator | Takara Bio | Cat# 631232 |
| E.Z.N.A. Endo-free plasmid mini kit II | Omega Bio-Tek | Cat# D6950-02 |
| Genelute HP Plasmid Maxiprep Kit | Sigma-Aldrich | Cat# NA0310-1KT |
| **Deposited Data** | | |
| Unprocessed IMF and WB images | Mendeley Data | http://dx.doi.org/10.17632/rt6y73mrb5.1 |
| **Experimental Models: Cell Lines** | | |
| HAP1 | Laboratory of Joseph Puglisi, Stanford Unviersity | N/A |
| U2OS | Laboratory of Dyche Mullins, UCSF | N/A |
| **Oligonucleotides** | | |
| Sequencing primer FH273: CAAGGCTGTTAGAGAGATAATTGGA | This study | N/A |
| Amplify region around FBXO42 genomic DNA-F: CATTTGGGAGCTAGGTAGGCTATTC TC | This study | N/A |
| Amplify region around FBXO42 genomic DNA-R: CACTGGCTTAGCACATGGAATTG | This study | N/A |
| Universal forward primer for amplification of sgRNA library: TACATCCTGGTTACTTGGC | This study | N/A |
| Universal reverse primer for amplification of sgRNA library: TGTCGTACCGTCTCCAAAC | This study | N/A |

| **Recombinant DNA** | | |
|---|---|---|
| **Reagent or Resource** | **Source** | **Identifier** |
| pCMV-VSV-G | Addgene | Cat#8454 |
| psPAX2 | Addgene | Cat#12260 |
| pMD2.G | Addgene / Davide Ruggero Lab | Cat#12259 / N/A |
| pLKO.1 FBXO42-1:: CCGGCCATCAGTGTTATCATGGTTT CTCGAGAAACCATGATAACACTGAT GGTTTTTTG | Sigma Mission shRNA | Glycerol Stock; TRCN0000134822 |
| TRC2-pLKO FBXO42-2: CCGGTAGATGATGCAACTATCTTAA CTCGAGTTAAGATAGTTGCATCATC TATTTTTG | Sigma Mission shRNA | Glycerol Stock; TRCN0000285999 |
| TRC2-pLKO FBXW7: CCGGCTAGAAAGGAACTGCAATAATCT CGAGATTATTGCAGTTCCTTTCTAGTTT TTG | Sigma Mission shRNA | Glycerol Stock; TRCN0000355644 |
| TRC2-pLKO BIRC6: CCGGCCCGTCAGTAGTGCGGTAAATC TCGAGATTTACCGCACTACTGACGGGT TTTTG | Sigma Mission shRNA | Glycerol stock; TRCN0000364501 |
| pLKO.1 FBXO8: CCGGGAGAGTATCTTGAAACTCTTA CTCGAGTAAGAGTTTCAAGATACTC TCTTTTTG | Sigma Mission shRNA | Glycerol stock; TRCN0000034316 |
| TRC2-pLKO ZBTB11: CCGGTAGATCGATCCCGTCCAATATCT CGAGATATTGGACGGGATCGATCTATT TTTG | Sigma Mission shRNA | Glycerol stock; TRCN0000376563 |
| Non-mammalian shRNA control: CAACAAGATGAAGAGCACCAA | Sigma Mission shRNA | SHC002 |
| **Software and Algorithms** | | |
| FIJI (ImageJ) | Schindelin et al., 2012 | https://imagej.net/Fiji |
| mhorlbeck/Screen processing | Horlbeck et al., 2016 *eLife* | https://github.com/mhorlbeck/ScreenProcessing |
| MAGeCK v.0.5.9.2 | Li et al. 2014 *Genome Biology* | https://sourceforge.net/p/mageck/wiki/Home/ |

| Software and Algorithms | | |
|---|---|---|
| **Reagent or Resource** | **Source** | **Identifier** |
| Canopy v.2.1.3.3542 | Enthought Inc. | https://store.enthought.com/downloads/ |
| TextWrangler v.5.5.2 | Bare Bones Software | https://www.barebones.com/products/textwrangler/download.html |
| FlowJo v.10.0.8 | Beckton, Dickinson and Company | https://www.flowjo.com |
| ImageStudioLite v.5.2.5 | Li-Cor Biosciences | https://www.licor.com/bio/image-studio-lite/ |
| Gene Cluster 3.0 | Stanford University, University of Tokyo | http://bonsai.hgc.jp/~mdehoon/software/cluster/software.htm |
| Java TreeView v.1.1.6r6 | Alok J. Saldanha | http://jtreeview.sourceforge.net/ |

**Supplementary File 1.S1. Targets and sgRNAs used in the CRISPR-Cas9 screen**
The first tab ("Target list") lists all genes targeted in the UPS CRISPR-Cas9 screen, grouped by type (F-box, RING, HECT, etc.), as well as non-targeting controls (CTRL00001-CTRL00082), and the twenty non-expressed genes (targeting controls). The second tab ("sgRNA sequences") lists all 6,306 sgRNA sequences used in the screen. For each gene, sgRNAs one through seven were selected from a previously published whole-genome essentiality screen (Wang et al., 2015), and sgRNAs eight and nine were designed to target the key catalytic or binding regions of each protein (this study). Non-targeting control sgRNAs represent a sub-set of the previously published list (Wang et al., 2015). Twenty non-expressed genes were selected as additional controls and were targeted with three sgRNAs each for a total of 60 targeting control sgRNAs (Wang et al., 2015).

**Supplementary File 1.S2. Illumina sequencing primers and barcodes used**
List of the 96 x 5'Illumina sequencing primers, each containing a unique six nucleotide barcode, with half annealing upstream of the sgRNA integration site (Set A), and half annealing downstream of the integration site (Set B). Also listed are the two 3' Illumina primers (for Set A and Set B), the 5' sequencing primer, and the 3' sequencing primer. A standard indexing primer was provided by the UCSF Center for Advanced Technology, which performed the sequencing.

**Supplementary File 1.S3. Inhibitors, targets, and doses used in the screen and validation experiments**
The 41 compounds used in the CRISPR-Cas9 screen including target, primary mechanism of action, and dosage information. In cases where the dose appeared too strong during the experiment, the dose was reduced as indicated for all replicates at the same time point.

**Supplementary File 1.S4. Mini-pools of sgRNAs used in GFP/BFP validation experiments**
Lists of the sgRNAs used in the GFP/BFP validation assays. A subset of the nine sgRNAs per gene in the screening library were selected for use in the validation assays based on performance in the screen.

**Supplementary File 1.S5. Primers used to confirm mutation of *FBXO42*, *HUWE1*, *RNF19A*, *UBE3D*, *UBE4B*, and *HERC2***

## MATERIALS & METHODS

### EXPERIMENTAL MODEL AND SUBJECT DETAILS

#### Cell Lines and Culture Conditions

HAP1 cells (male) were grown in IMDM supplemented with 10% tetracycline-free FBS and 4mM L-glutamine, without antibiotics. U2OS cells (female) were grown in DMEM supplemented with 10% FBS and 2mM L-glutamine, without antibiotics. HEK293T cells (female) used to package lentivirus were grown in DMEM supplemented with 10% FBS and 2mM L-glutamine, without antibiotics. All cells were grown at 37ºC and 8% $CO_2$ in standard tissue culture incubators.

Our laboratory conducts regular mycoplasma testing of cultured cells with the MycoAlert Mycoplasma Detection kit (Lonza), and no mycoplasma contamination of any cell line was detected during this study.

### METHOD DETAILS

#### CRISPR-Cas9 sgRNA design

A list of nearly all human E3s as well as the non-essential DUBs was compiled by referencing previous work (Li et al., 2008; Liu et al., 2019) and searching protein sequence databases for other proteins containing predicted E3 domains (e.g. RING domains) (Supplementary File 1.S1). In total, the list includes 629 E3 catalytic components, substrate binding modules, and structural components, as well as 56 DUBs. For each gene, seven effective sgRNAs were selected from the genome-wide essentiality screen conducted by Wang et al. (Wang et al., 2015) (sgRNAs one through seven), and two new domain-specific sgRNAs were designed (sgRNAs

eight and nine) (described in further detail below). As controls, 81 non-targeting and 60 targeting sgRNAs (with three sgRNAs targeting each of 20 genes predicted to not be expressed in most cells, including olfactory receptors and testes-specific genes) were also included (Wang et al., 2015), for a total library of 6,306 sgRNAs (Supplementary File 1.S1).

***Domain-specific sgRNA design***

Based upon statistics alone, one-third of the time, a double-strand break generated by Cas9 will be repaired with an in-frame insertion or deletion, and unless such an indel disrupts residues that are key to the function of the protein or is so large as to significantly alter the structure, the mutated protein may still be functional. This would tend to limit the sensitivity of a CRISPR-Cas9 screen, since at most two thirds of modified cells will have a non-functional protein, assuming the sgRNA targets near the 5' end of the gene. Theoretically, sgRNAs that precisely target codons for key catalytic or binding residues, rather than just the 5' end of the gene, would be more likely to yield a non-functional protein, even if the break is repaired with an in-frame indel (Shi et al., 2015). This strategy is of course limited by the availability of PAM sequences in the desired region and depends on there being unique sequences to target, which can be difficult when targeting a highly conserved region.

Two domain-specific sgRNAs were designed for each gene as follows, and using the previously available Feng Zhang lab online sgRNA design tool to predict and avoid off-target effects. For F-box proteins (CUL1 substrate receptors), which have a roughly 40 amino acid F-box domain that binds SKP1, sgRNAs targeting structurally-defined SKP1 contact residues were designed (Schulman et al., 2000). For U-box proteins, sgRNAs targeting the RING-like U-box domain

responsible for E2 binding were designed (Koegl et al., 1999; Ohi et al., 2003). CUL4A/CUL4B substrate receptors (DCAFs) contact DDB1 through one or more of several motifs: an HLH motif, an HLH-like motif termed "CRBN-type binding", and DWxR motifs within a WD40 domain (Fischer et al., 2011, 2014; Gérard et al., 2014; Li et al., 2010). For some DCAFs, the crucial DDB1-binding motifs have been identified, but for others, these motifs had to be computationally predicted based on sequence alignments to well-characterized members of the group. Subsequently, sgRNAs targeting the most important motif for binding (or the motif predicted to be the most important based on alignment) were designed. For CUL3 substrate receptors, which interact with CUL3 via BTB domains and in particular the 3-box motif within the BTB, sgRNAs targeting the BTB domain were designed (Canning et al., 2013). Some, presumably monomeric, CUL3 receptors contain two BTB domains, and in these cases, only one of the BTB domains was targeted. For CUL2/5 substrate receptors, which contact TCEB1/TCEB2 via a SOCS-box or VHL domain, sgRNAs targeting close to the beginning of the domain were designed since the main point of contact occurs in the first 6-10 amino acids of the domain (Cai and Yang, 2016; Stebbins et al., 1999). For the cullins themselves, sgRNAs targeting the cullin-RBX1/RBX2 contact domain, and specifically the S2 strand when possible, were designed (Zheng et al., 2002). For HECT E3s, which contain both E2-binding regions and catalytic clefts containing the conserved, catalytic cysteine, sgRNAs targeting the catalytic cleft were designed. In some cases, candidate sgRNAs targeting the catalytic cleft had many predicted off-target sites, so the E2-binding region was targeted instead. For RING finger E3s, sgRNAs targeting the RING domain and, when possible, the key cysteine or histidine residues involved in zinc coordination were designed (Freemont, 1993; Lorick et al., 1999). For RBRs, sgRNAs targeting the RING2 catalytic cysteine were designed, and when this was not possible,

sgRNAs targeting the E2-binding RING1 were designed (Bijlmakers et al., 2016; Spratt et al., 2014). Finally, for MINDY, USP, OTU, UCH, and Josephin DUBs, sgRNAs targeting as close as possible to the catalytic cysteine were designed (Abdul Rehman et al., 2016; Komander et al., 2009). In some cases, the catalytic cysteines are not annotated, so they were predicted based on sequence alignments and identification of the most likely residue based on conservation across a DUB family. For the JAMM/MPN+ DUBs, sgRNAs targeting the zinc coordination region (JAMM motif) were designed (Sato et al., 2008).

**CRISPR-Cas9 sgRNA cloning**

To amplify the sgRNAs, oligos containing universal forward and reverse primer-binding sites surrounding the sgRNA and flanking BsmBI sites were designed such that all 6,306 different sgRNAs could be amplified simultaneously from the source pool. The BsmBI sites enabled restriction-ligation cloning of digested PCR products. The oligos additionally contained gene-specific forward primer-binding sites to enable specific amplification of the nine sgRNAs for a gene of interest. To increase gene-specific primer specificity, a published list of orthogonal primers was analyzed to find a subset with the most dissimilar sequences possible, and these were used in constructing the sgRNA oligos and complementary primers (Xu et al., 2009). Oligos were 82 bp long and were synthesized in a pooled-format by CustomArray, Inc. Universal and gene-specific primers were synthesized by Integrated DNA Technologies.

A modified version of the lentiGuide-Puro vector (Addgene, plasmid #52963) (Sanjana et al., 2014) was generated with Sbf1 restriction sites flanking the sgRNA region for optional extraction from the genome during sequencing library preparation. The plasmid was digested

with BsmBI in NEB buffer 3.1 and gel purified. sgRNAs were amplified from the pool using the universal forward and reverse primers, purified with a Qiagen MinElute PCR cleanup kit, digested with Esp3I (an isoschizomer of BsmBI, which in our hands much more efficiently digested the small sgRNA-containing PCR products), and gel purified from 20% acrylamide gels following standard protocols. The digested vector and insert were then ligated together with T4 DNA ligase at a molar ratio of 1:2 vector:insert, and electroporated into MegaX electrocompetent *E.coli* at 1800V in an Eppendorf Electroporator 2510. In order to maintain at least 200-fold coverage and to maintain equal representation of each sgRNA in the library, electroporated *E. coli* were plated onto 22x15cm petri dishes containing LB agar+carbenicillin (75µg/mL) such that single colonies would be distinguishable and of roughly equal size. Approximately $2x10^6$ colonies were recovered, representing over 300-fold coverage of the library. Colonies were scraped from the plate, pooled, grown for about 2 hours at 37ºC in fresh LB+carbenicillin, then spun and pelleted. Plasmid DNA was extracted using the GenElute HP Plasmid MaxiPrep kit (Sigma). To check the quality of the library, 20 individual colonies from the MegaX electroporation were isolated, plasmid DNA was extracted, and sgRNA sequences were checked by Sanger sequencing. 17/20 (85%) were exact matches to 17 different sgRNAs in the library, which is consistent with normal library quality. A comprehensive quality control of the library was later done by deep sequencing (see peer-reviewed publication).

**HAP1-Cas9 clone generation**

HAP1 clones expressing a TRE (tetracycline response element), a doxycycline-inducible TRE3G driven 3xFlag-Cas9, and Blasticidin S deaminase were generated by integration of a modified version of pAAVS1-PDi-CRISPRn (Mandegar et al., 2016). The puromycin N-acetyltransferase

(PAC) gene in pAAVS1-PDi-CRISPRn was replaced with a Blasticidin S deaminase gene so that sgRNAs could be marked with PAC and selected. Initially, forward and reverse TALENs were used in an attempt to integrate the construct into the "safe harbor" AAVS1 locus as described in Mandegar et al., 2016, but recovered clones that had the integration at this site appeared to rapidly silence Cas9, suggesting AAVS1 is not a "safe harbor" in HAP1 cells. Other clones with stable Cas9 expression appeared to have the construct integrated elsewhere in the genome, and these were used for the CRISPR-Cas9 screen. Cells were co-transfected with pAAVS1-PDi-CRISPRn-Blast, AAVS1 TALEN F, and AAVS1 TALEN R with FuGENE HD transfection reagent following standard protocols and using a 3µL FuGENE to 1µg DNA ratio. The next day, cells were split, and two days after the transfection, cells were treated with Blasticidin S HCL at 10µg/mL. After six days of selection with Blasticidin, negative control wells were dead, transfected wells were taken off Blasticidin, colonies were allowed to grow up, then clones were isolated and analyzed for doxycycline-inducible Cas9 expression (with three days of 1µg/mL doxycycline treatment) over several weeks in culture by Western blot. In general, HAP1-Cas9 clones were grown in 10µg/mL Blasticidin to maintain selection for integrated Cas9. HAP1 cells diploidized rapidly into stable diploid lines.

**CRISPR-Cas9 screen of the ubiquitin pathway**

***Compound concentration determination***

To select the dose of each compound used in the screen, HAP1-Cas9 cells were initially seeded at a density of 6 million cells per well in 6-well plates and grown in the presence or absence of each compound over a range of 12 or more doses. Cells were split into fresh compound every two days for a period of eight days and observations of cell confluency and apparent death were

made every two days. Doubling time was calculated for each dose, and a dose that inhibited growth to about 70% of untreated controls was selected for the screen.

For the cell cycle profile and immunofluorescence experiments carried out in U2OS cells, $GFP^+$ U2OS used were used to determine the dose of BI-2536, TAK-901 and colchicine as described above.

***Lentivirus production & infection of HAP1-Cas9 clones***

293T cells in 15cm dishes at 60-70% confluency were transfected with 11.25µg of the sgRNA library, 6.75µg psPAX2, and 3.38µg VSVG using 64.1µL FuGENE HD (3µL FuGENE:1µg DNA) following standard protocols. 5 to 6hr after transfection, the medium was replaced with 10mL IMDM, and 24h after transfection, media containing viral particles was harvested, filtered through a 0.45µm SFCA filter, diluted with warm IMDM, supplemented with 8µg/mL polybrene, and used to infect HAP1-Cas9 clones in 15cm dishes at an infection ratio of 1:6 (one 15cm dish worth of lentiviral media to six 15cm dishes of HAP1 cells). With this library and protocol, this yields an effective MOI of 0.3-0.5. In order to have at least 1,000-fold coverage of every sgRNA in the library for each replicate of the screen, three 15cm plates of HAP1-Cas9 cells at 70-80% confluency were infected. Each 15cm of HAP1 contains approximately $7.5x10^7$ cells. 24h after start of infection, media containing virus was removed by aspiration and replaced with fresh IMDM. 24h later, infected cells were split into fresh IMDM with 1µg/mL puromycin to select for sgRNA integration. In parallel, un-infected cells were split into puromycin. Cells were given fresh media with puromycin every day for a total of four days, at which point all cells in the un-infected dish were dead. Cells were given one day of recovery,

after which one dish of each replicate was collected as the "pre-dox" sample for sequencing to determine the initial sgRNA abundance. Remaining dishes were split into fresh IMDM with 1μg/mL doxycycline to induce Cas9 expression. Cells were given fresh doxycycline every day for a total of three days. Throughout the puromycin selection and doxycycline treatment, cells were split when necessary (always maintaining 1,000-fold sgRNA coverage) and expanded so that there would be enough cells on day zero, when treatment with each compound began. Cells were given one day of recovery after doxycycline, then cells were split into one of the 41 compounds.

***Pooled CRISPR-Cas9 screen***

After infection, selection, and Cas9 induction, as described above, cells were split into media with or without one of the 41 compounds, seeding enough cells for the desired 1,000-fold sgRNA coverage. Cell confluency and death were visually inspected every two days, then cells were split into fresh media with the appropriate compound and at the appropriate split ratio to maintain >1,000-fold sgRNA coverage. Excess cells from splitting were collected at intermediate time points, following standard protocols, and all cells were collected on day 8, the final time point. For each replicate of each compound, one 15cm plate was used for every time point. Some compounds had a stronger effect of the cells in the context of sgRNA library infection and Cas9-induction than they did in trial compound dosing experiments in 6-well plates. In these cases, the compound dose was adjusted during the screen time course for all replicates in order to ensure sufficient cell survival to the end of the experiment (Supplementary File 1.S3).

*Next generation sequencing library preparation*

Genomic DNA was extracted from cell pellets collected from the screen using a Nucleospin blood L midi kit (Machery Nagel), following standard protocols, performing an extra dry spin after the second wash in buffer BQ2, and eluting with 340µL of EB. For each sample, three 100µL PCRs each with 10µg of gDNA were carried out to amplify the sgRNA and to append barcodes and Illumina sequencing adapters, with each replicate of each compound having its own barcode. Given the size of our library, only one PCR, rather than two sequential PCRs as described previously (Han et al., 2017), were required to prepare samples for sequencing. One of 96 oligos containing a unique hexamer barcode, the 5' Illumina sequencing adapter, and a primer designed to the constant region outside of the sgRNA were paired with one of two common 3' primers containing the 3' Illumina adapter (Supplementary File 1.S2). A small fraction of each individual PCR was run on a 1.4% agarose gel to check for successful amplification. Careful PCR practices including negative control reactions were employed throughout to avoid cross-contamination of samples. To achieve 1,000-fold coverage during deep sequencing, 45 or fewer samples with unique barcodes were pooled for each sequencing lane (average PF reads per lane ~$3.9x10^8$). The pooled samples were gel purified following standard protocols, then deep sequenced on the Illumina HiSeq 4000 with single end, 50 base reads (UCSF Center for Advanced Technology) using common 3' and 5'sequencing primers and an indexing primer provided by the core facility (Supplementary File 1.S2).

**Clonal mutant HAP1 cell line generation**

To generate each clonal mutant cell line of candidate mitotic E3s (FBXO42, HUWE1, UBE3D, HERC2, UBE3D, and RNF19A), one of the HAP1-Cas9 clones was infected at low MOI

following standard protocols with a modified lentiGuidePuro vector containing one sgRNA. Integration of the sgRNA was selected for with 1μg/mL puromycin for four days, cells were taken off puromycin for one day, then Cas9 was induced with 1μg/mL doxycycline hyclate for three days. Cells were thoroughly trypsinized to yield single cells, plated at very low confluency in 10cm dishes, allowed to grow to up to small colonies, and colonies were isolated by picking and plating into individual wells of TC-treated plates. Isolated colonies were screened for mutation of the targeted gene by PCR of the region surrounding the Cas9 cut site, followed by Sanger sequencing of the purified PCR product. For proteins with available antibodies, promising clones were also screened for protein depletion by Western blot. Note that over many weeks in culture, some E3 mutant clones showed signs of slight protein levels, suggesting that rearrangements occurred and were selected for since some of the mutations resulted in slower growth.

**Internally controlled, competitive growth assays (GFP/BFP and GFP+/–)**

One of the HAP1-Cas9 clones used in the CRISPR-Cas9 screen was additionally modified to constitutively express GFP by transfection and random integration of GFP-IRES-Hygro (Addgene #64375). Cells were transfected with FuGENE HD transfection reagent, following standard protocol, then selected for ten days in 250μg/mL Hygromycin B, sorted by FACS for individual cells that highly expressed GFP, allowed to expand, then checked for sustained bright GFP by flow cytometry. Several consistently bright clones were isolated, and two of these were used for the internally controlled, competitive growth assays. These clones were maintained on 10μg/mL Blasticidin and 250μg/mL Hygromycin B. Constitutively BFP-expressing HAP1 cells were generated by lentiviral infection of wild type HAP1 cells at a low MOI with eBFP2-Blast-

HM following standard protocols, selection with 10μg/mL Blasticidin for ten days, and sorting by FACS for individual cells that highly expressed BFP. Once clonal populations grew up, they were checked again for BFP expression by flow cytometry. Several consistently bright clones were isolated, and two of these were used for the internally controlled, competitive growth assays. These clones were maintained on 10μg/mL Blasticidin.

sgRNAs were isolated from the library oligo pool by PCR with the correct gene-specific forward primer and the universal reverse primer. PCR products were purified with the Qiagen MinElute kit, digested with Esp3I, and isopropanol precipitated following standard protocols. The lentiGuide-Puro vector was digested with BsmBI in NEB buffer 3.1 and gel purified. The digested vector and insert were then ligated together with T4 DNA ligase at a molar ratio of approximately 1:9 vector:insert and transformed into XL10 Gold *E. coli*. Colonies were prepped for Sanger sequencing and transfection using an E.Z.N.A. Endo Free Plasmid Mini Kit II (Omega Bio-Tek).

For GFP/BFP competitive growth assays, two duplicates of GFP/BFP cell mixtures (four total replicates) were made at roughly equal ratios of GFP to BFP. Mixtures were infected at high MOI with pools of 2-4 sgRNAs targeting one gene (or with 11 targeting control sgRNAs for the control experiment) (Supplementary File 1.S4), treated with 1μg/mL puromycin for four days and 1μg/mL doxycycline for three days to select for sgRNA integration and to induce Cas9 expression, then split into media with or without one of several compounds every two days for eight days. The GFP/BFP ratio was measured by flow cytometry every two days, starting on day zero when compounds were added. FlowJo was used for data analysis, and each ratio of GFP to

BFP was normalized to the day zero ratio, and subsequently to the matched untreated ratio at each time point. Cyotochalasin D served as a negative control compound for most experiments.

For HAP1 GFP+/– competitive growth assays, clonal E3 mutant cells were mixed with one of the bright $GFP^+$ clones at roughly equal $GFP^+$ to $GFP^–$ ratios, then split into media with or without one of several compounds and analyzed by flow cytometry as described above.

A pool of U2OS cells expressing GFP was generated by random integration of GFP-IRES-Hygro (Addgene #64375) and selection with 125µg/mL Hygromycin B following standard protocols. Flow cytometry analysis of the selected pool showed approximately 98% of cells expressed GFP and were very bright, and this profile remained the same over many weeks in culture with or without 125µg/mL Hygromycin B. Pools of U2OS $GFP^–$ cells with integrated shRNAs were generated as described below: FBXO42-1, FBXO42-2, FBXW7, BIRC6, FBXO8, and ZBTB11, Control-1; and one U2OS $GFP^+$ pool with a control shRNA was generated: Control-2. FBXO42-1: TRCN0000134822; FBXO42-2: TRCN0000285999; FBXW7: TRCN0000355644; BIRC6: TRCN0000364501; FBXO8: TRCN0000034316; ZBTB11: TRCN0000376563; Control-1: U2OS $GFP^–$ with SHC002; Control-2: U2OS $GFP^+$ pool with SHC002 (Sigma, Mission shRNA). U2OS GFP+/– experiments were conducted similarly to the HAP1 GFP+/– assays, with the addition of 2µg/mL puromycin throughout the experiment to maintain selection for integrated shRNAs.

**Western blotting**

For Western blots, cell pellets were lysed in 1xRIPA buffer with protease and phosphatase inhibitors for 30 minutes on ice with two rounds of 15 second vortexing, insoluble material was spun out, relative protein concentration was determined by BCA (Pierce), and samples were normalized to one-another by addition of 1xRIPA with inhibitors. SDS sample buffer with 100mM DTT was added to samples, which were then loaded onto 4-20% Criterion Tris-HCl Protein gels (Bio-Rad) and separated by electrophoresis at 80-120 V for 2-3h. Proteins were transferred and immobilized onto a nitrocellulose membrane (GE Healthcare) by electrophoresis for 4h at 0.4A (4°C) in standard transfer buffer containing 20% methanol. Membranes were blocked in either 5 % non-fat dry milk in PBS-T or Odyssey Blocking Buffer (PBS) (LICOR), for HRP-conjugated and fluorescent secondary antibodies, respectively. All mouse primary antibodies were probed with goat-anti-mouse 800 CW LICOR secondary antibodies, rabbit-anti-HUWE1 was probed with Protein A-HRP, and all other rabbit primary antibodies were probed with goat-anti-rabbit HRP secondary antibody. Chemiluminescent and fluorescent signals were visualized with an Odyssey FC imager (LICOR).

***Antibodies for Western Blotting:***

1:250 rabbit-anti-UBE3D (abcam), 1:1000 rabbit-anti-FBXO42 (AbClonal), 1:750 rabbit-anti-FBXO42 (Avivia), 1:1,000 rabbit-anti-HUWE1 (Simon Wing lab), 1:2,000 mouse-anti-FLAG (Sigma), 1:1,000 mouse-anti-vinculin (Sigma), 1:5,000 mouse-anti-B-actin (Sigma), 1:1,000 rabbit anti-FBXW7 (Bethyl A301-720A), 1:1,000 rabbit anti-BIRC6 (Cell Signaling), 1:1,000 rabbit anti-ZBTB11 (Bethyl), 1:5,000 goat-anti-mouse HRP conjugate (Bio-Rad),

1:5,000 goat-anti-rabbit GFP conjugate (Bio-Rad), 1:5,000 goat-anti-mouse 800CW (LICOR), 1:10,000 Protein A-HRP conjugate (Bio-Rad).

**Cell cycle analysis**

Cells were treated with inhibitor 24h after plating, then harvested 10 or 24h later by trypsinization, washed twice with cold 1X PBS, fixed by dropwise addition of ice-cold 70% ethanol, and incubated overnight (4ºC). Fixed samples were washed twice with 1X PBS + 1% BSA prior to RNA degradation using 1mg/mL RNase A and DNA labeling with 50 µg/mL propidium iodide for 30-45 minutes at 37ºC. DNA content was measured on a SH800 cell sorter (SONY) or a BD FACSVerse flow cytometer (BD Biosciences), and data were analyzed using FlowJo.

**shRNA experiments**

Control (SHC002), FBXO42, FBXW7, BIRC6, FBXO8, and ZBTB11 shRNAs containing a Puromycin N-acetyltransferase gene (Sigma, Mission shRNA) were integrated into U2OS cells by infection. Lentivirus was made by transfecting 293T cells at 60-70% confluency in 10cm dishes with 300ng pMD2.G, 600ng psPAX2, 1µg shRNA construct, and FuGENE HD transfection reagent (3µl FuGENE HD:1µg plasmid DNA) following standard protocols. Media was replaced with 5mL warm DMEM 5 to 6hr after transfection. 24h after transfection, media containing viral particles was harvested, filtered through a 0.45µm SFCA filter, combined with 1.5mL LentiX concentrator (Takara Bio) per 5mL viral media, rotated for 30-60 minutes at 4ºC, and pelleted at 1,500xg for 45 minutes at 4ºC. The viral pellet was thoroughly resuspended in 1mL warm DMEM, then used to infect one well of a 6-well dish of wild type U2OS cells or the

U2OS-GFP$^+$ pool at 80% confluency. After 24h of infection, viral media was replaced with fresh DMEM for 24h, then cells were split into fresh DMEM with 2μg/mL puromycin. In parallel, un-infected cells were treated with puromycin. Cells were given fresh media with puromycin every day for a total of four days, at which point the cells in un-infected wells were dead. During selection, cells were split as necessary. Knockdown of FBXO42, BIRC6, and ZBTB11 were confirmed by Western blot, while knockdown of FBXW7 was confirmed by immunoprecipitation using rabbit anti-FBXW7 (Bethyl A301-721A) and Protein A Dynabeads using 0.1% NP-40 buffer and following standard procedures. For competitive growth assays, propidium iodide-based cell cycle analysis, and immunofluorescence, shRNA U2OS pools were grown in 2μg/mL puromycin to maintain selection for the integrated shRNA (loss of silencing was observed without puromycin). U2OS-GFP$^+$ pools with integrated SHC002 were grown in both puromycin and 125μg/mL Hygromycin B to maintain selection for GFP.

**Immunofluorescence and Microscopy**

Cells were seeded on coverslips coated with 5μg/mL fibronectin (EMD Millipore). After 24h of growth, BI-2536 was added for 24h, cells were collected and coverslips were fixed with -20°C methanol + 5mM EGTA for 1 minute or 4% formaldehyde in PBS for 10 min at room temperature. Coverslips were washed in TBS-0.05% Triton three times for 5 min and blocked with 0.05% TBS-T supplemented with 2% BSA (Sigma-Aldrich) for 1.5h at room temperature. Coverslips were incubated with a polyclonal anti-tubulin (DM1α) Alexa Fluor 488 conjugate (1:50, Cell Signaling Technology) for 2h at room temperature. Coverslips were washed twice with TBS-0.05% Triton for 5 min, and DNA was stained with 10μg/mL DAPI (Invitrogen) for 5 min at room temperature and mounted with vectashield mounting medium (LSBio) onto slides.

## QUANTIFICATION AND STATISTICAL ANALYSIS

### CRISPR-Cas9 screen data analysis

#### *Sequence alignment & data analysis*

Deep sequencing runs achieved an average of $3.9x10^8$ PF reads and 20,000 MB per lane, and with 45 or fewer barcodes per lane, average sgRNA coverage was over 1,300-fold. Raw sequencing reads were sorted by barcode then trimmed and aligned to the E3 and DUB sgRNA library using TextWrangler, Max Horlbeck's Screen Processing code (Horlbeck et al., 2016), and Canopy platform for Python (see peer-reviewed publication). sgRNAs with less than 100 aligned counts in one or more replicates were excluded from further analysis. Three genes, DCAF12L1, MEX3B, and RFPL2, were excluded completely from further analysis because five or more of their sgRNAs had aligned counts below 100. TRIM64 was also removed entirely because its first seven sgRNAs were identical to those of DCAF7, indicating an error was made earlier in sgRNA library design.

Counts were then normalized to the total number of counts per barcode, indicating the fractional sgRNA abundance for each sample, then normalized to pre-dox values to reveal the change in sgRNA abundance from just after sgRNA integration (pre-dox) to after Cas9 induction (day 8 samples) (see peer-reviewed publication). To determine the effect of growth in the test compounds, values were finally normalized to matched untreated values. The median of nine sgRNAs per gene was calculated, the medians of all replicates for each compound were calculated, and the final values were Log2 transformed (see peer-reviewed publication). For the 81 non-targeting control sgRNAs, the median of groups of nine were calculated for nine final values (called CTRL00001, CTRL00010, CTRL00019, CTRL00028, CTRL00037, CTRL00046,

CTRL00055, CTRL00064, and CTRL00073). For the 60 targeting control sgRNAs against 20 genes, the median of groups of nine were calculated for seven final values (Targeting1-7, with Targeting7 being the median of the last six sgRNAs instead of nine). Pearson correlation coefficients were calculated for the three replicates of each compound (see peer-reviewed publication). This analysis revealed that for two of the 41 compounds (bortezomib and vismodegib), one of the three replicates was an extreme outlier having no correlation with the other two replicates, so these replicates were excluded from further analysis. An additional compound, RO-3306 had one replicate that was not strongly correlated with the other two replicates (PCC=0.36), but this replicate was included in analysis because it was still weakly correlated. For three of the 41 compounds (TTFA, leptomycin B, and pravastatin), one of the three replicates were lost during the experiment due to the compound concentration being too high, despite downward dosage adjustment during the time course. After these adjustments, the average PCC between replicates for all compounds was 0.67.

Data were further analyzed by calculating four standard deviations from the mean of the targeting control sgRNAs across all compounds ($\mu$=0.004, Std Dev=0.07) to establish Log2 fold change cut-offs for significance of ± 0.3. Four standard deviations from the mean of the targeting controls is more precisely 0.29 and -0.28, but the cut-offs were rounded to ± 0.3 for simplicity. A reproducibility cut-off was set at p-value ≤0.01 (equivalent to –Log10(p-value) ≥2), and p-values were calculated using all 27 sgRNAs per gene (from three replicates) or 18 sgRNAs per gene (in cases where only two replicates were included in analysis).

To calculate FDRs, the MAGeCK analysis was performed as previously described (Li et al., 2014) using MAGeCK version 0.5.9.2. Briefly, the sgRNA read count tables from next-generation sequencing were used as input and the *mageck test* command with *--control-sgrna* option was performed for each drug treatment.

***Clustering and visualization***

Screen data were clustered using Cluster 3.0 software, using unbiased, hierarchical clustering (uncentered) with average linkages. Data were visualized with Java TreeView v1.1.6r4.

**Additional statistical analyses**

For all growth assays, cell cycle analyses, and microscopy, data are represented as the mean ± SEM. Differences between two sample groups were determined by standard two-tailed equal or unequal variance t-tests, with p-values indicated in the figure legends. Figure legends indicate the number of replicates for each experiment.

**Image acquisition and analysis**

Widefield images were acquired on an inverted Nikon Ti-E with a fully automated stage (Nikon), equipped with a sCMOS DS-Qi2 (Nikon), Sutter LS lamp with filter wheel and shutter (Sutter Instruments), and an A 5-band FF408/504/581/667/762 dichroic (Semrock). For immunofluorescence and quantification, images were captured with a Plan Apo VC 60x/1.4 oil lens using a 0.3µm Z-step (Nikon). Dual color images with DAPI/Alexa Fluor 488 anti-Tubulin or DAPI/Alexa Fluor 555 anti-Tubulin were captured sequentially using excitation filters,

387/11x, 485/20x, and 560/25x, and emission filters 440/40m, 525/30m, and 607/36m, for DAPI, AlexaFluor 488, and AlexaFluor 555, respectively.

For high-resolution monopolar spindle images, an inverted Nikon Ti-E (Nikon) equipped with a motorized piezo z-stage (Prior), a CSU-22 spinning disk containing dichroics 405/491/561/640 (Yokagawa), an EMCCD Evolve Delta (Photometrics) camera, Sutter Emission wheel controlled by Lambda 10-B (Sutter Instruments), and Orbis lasers 405/488/561/647nm (Coherent) was used. Images were taken sequentially with a Plan Apo VC 100x/1.4 oil lens (Nikon) using a 0.3µm Z-stack, by exciting with a 405nm or 488nm laser with emission filters ET460/50m and ET525/50m (Chroma) in the camera light path for DAPI or Alexa Fluor 488 anti-Tubulin, respectively.

For quantitative analysis, all images were captured using identical conditions and are displayed following identical settings using ImageJ software. In all cases, to quantify the proportion of cells in mitosis and the frequency of monopolar spindles, images were captured from three independent experiments. We performed a blinded analysis of the images, characterizing each cell line with or without BI-2536 according to two different microtubule morphology categories: interphase cells and mitotic cells. The mitotic cell category was further divided into normal mitotic cells at any stage (from prometaphase to cytokinesis) and monopolar spindles. A minimum of 250 mitotic cells were counted per replicate. Differences between two groups of data were analyzed by two-tailed equal variance t-tests.

## DATA AND CODE AVAILABILITY

CRISPR-Cas9 screen data analysis code by Max Horlbeck is available on GitHub: https://github.com/mhorlbeck/ScreenProcessing (Horlbeck et al., 2016), and MAGeCK data analysis code is available at: https://sourceforge.net/p/mageck/wiki/Home/ (Li et al., 2014).

Aligned deep sequencing read counts are available in the peer-reviewed publication.

Unprocessed microscopy images and western blots are available on Mendeley Data: https://data.mendeley.com/datasets/rt6y73mrb5/draft?a=f4b895a1-4104-4e7c-863b-24fb7e6bfcce

**Acknowledgements**

We thank members of the Toczyski, Dumont, Gilbert, Jura, Kampmann, McManus, and Morgan labs for helpful discussions. In addition, we would like to thank the Dumont lab and Sol Fereres for microscopy advice and Mary McMahon for suggestions in the early stages of establishing CRISPR-Cas9 methods in our laboratory. We acknowledge the generous gifts of the following reagents: HAP1 cells from the Puglisi laboratory (Stanford University); pAAVS-PDi-CRISPRn plasmid from Mo Mandegar, Conklin laboratory (UCSF); JG-231 from the Gestwicki laboratory (UCSF); and HUWE1 antibody ($\alpha$-LASU1) from Simon Wing lab (McGill University). This work was supported by an NIH grant (R35 GM118104 to D.P.T.), funding from the UCSF RAP program, the UCSF Program for Breakthrough Biomedical Research (funded in part by the Sandler Foundation), a National Cancer Institute Cancer Center Support grant (P30CA082103), the UCSF Center for Advanced Technology, and the UCSF Nikon Imaging Center.

## REFERENCES


Abdul Rehman, S.A., Kristariyanto, Y.A., Choi, S.-Y., Nkosi, P.J., Weidlich, S., Labib, K., Hofmann, K., and Kulathu, Y. (2016). MINDY-1 Is a Member of an Evolutionarily Conserved and Structurally Distinct New Family of Deubiquitinating Enzymes. Molecular Cell *63*, 146–155.

Al-Hakim, A.K., Bashkurov, M., Gingras, A.-C., Durocher, D., and Pelletier, L. (2012). Interaction Proteomics Identify NEURL4 and the HECT E3 Ligase HERC2 as Novel Modulators of Centrosome Architecture. Mol Cell Proteomics *11*.

Arnason, T., and Ellison, M.J. (1994). Stress resistance in Saccharomyces cerevisiae is strongly correlated with assembly of a novel type of multiubiquitin chain. Mol. Cell. Biol. *14*, 7876–7883.

Asamitsu, K., Tetsuka, T., Kanazawa, S., and Okamoto, T. (2003). RING Finger Protein AO7 Supports NF-κB-mediated Transcription by Interacting with the Transactivation Domain of the p65 Subunit. J. Biol. Chem. *278*, 26879–26887.

Ballinger, C.A., Connell, P., Wu, Y., Hu, Z., Thompson, L.J., Yin, L.-Y., and Patterson, C. (1999). Identification of CHIP, a Novel Tetratricopeptide Repeat-Containing Protein That Interacts with Heat Shock Proteins and Negatively Regulates Chaperone Functions. Mol. Cell. Biol. *19*, 4535–4545.

Bekker-Jensen, S., Danielsen, J.R., Fugger, K., Gromova, I., Nerstedt, A., Lukas, C., Bartek, J., Lukas, J., and Mailand, N. (2010). HERC2 coordinates ubiquitin-dependent assembly of DNA repair factors on damaged chromosomes. Nature Cell Biology *12*, 80–86.

Benanti, J.A., Cheung, S.K., Brady, M.C., and Toczyski, D.P. (2007). A proteomic screen reveals SCFGrr1 targets that regulate the glycolytic–gluconeogenic switch. Nat Cell Biol *9*, 1184–1191.

Bennett, E.J., Rush, J., Gygi, S.P., and Harper, J.W. (2010). Dynamics of cullin-RING ubiquitin ligase network revealed by systematic quantitative proteomics. Cell *143*, 951–965.

Bijlmakers, M.-J., Teixeira, J.M.C., Boer, R., Mayzel, M., Puig-Sàrries, P., Karlsson, G., Coll, M., Pons, M., and Crosas, B. (2016). A C2HC zinc finger is essential for the RING-E2 interaction of the ubiquitin ligase RNF125. Sci Rep *6*, 29232.

Blake, J.F., Xu, R., Bencsik, J.R., Xiao, D., Kallan, N.C., Schlachter, S., Mitchell, I.S., Spencer, K.L., Banka, A.L., Wallace, E.M., et al. (2012). Discovery and Preclinical Pharmacology of a Selective ATP-Competitive Akt Inhibitor (GDC-0068) for the Treatment of Human Tumors. J. Med. Chem. *55*, 8110–8127.

Brandman, O., Stewart-Ornstein, J., Wong, D., Larson, A., Williams, C.C., Li, G.-W., Zhou, S., King, D., Shen, P.S., Weibezahn, J., et al. (2012). A Ribosome-Bound Quality Control Complex Triggers Degradation of Nascent Peptides and Signals Translation Stress. Cell *151*, 1042–1054.

Brocker, C., Kuhlee, A., Gatsogiannis, C., kleine Balderhaar, H.J., Honscher, C., Engelbrecht-Vandre, S., Ungermann, C., and Raunser, S. (2012). Molecular architecture of the multisubunit homotypic fusion and vacuole protein sorting (HOPS) tethering complex. PNAS *109*, 1991–1996.

Cai, W., and Yang, H. (2016). The structure and regulation of Cullin 2 based E3 ubiquitin ligases and their biological functions. Cell Div *11*, 7.

Canning, P., Cooper, C.D.O., Krojer, T., Murray, J.W., Pike, A.C.W., Chaikuad, A., Keates, T., Thangaratnarajah, C., Hojzan, V., Marsden, B.D., et al. (2013). Structural Basis for Cul3 Protein Assembly with the BTB-Kelch Family of E3 Ubiquitin Ligases. J. Biol. Chem. *288*, 7803–7814.

Chau, V., Tobias, J.W., Bachmair, A., Marriott, D., Ecker, D.J., Gonda, D.K., and Varshavsky, A. (1989). A multiubiquitin chain is confined to specific lysine in a targeted short-lived protein. Science *243*, 1576–1583.

Ciechanover, A., Heller, H., Elias, S., Haas, A.L., and Hershko, A. (1980). ATP-dependent conjugation of reticulocyte proteins with the polypeptide required for protein degradation. PNAS *77*, 1365–1368.

Clague, M.J., Heride, C., and Urbé, S. (2015). The demographics of the ubiquitin system. Trends in Cell Biology *25*, 417–426.

Deshaies, R.J., and Joazeiro, C.A.P. (2009). RING Domain E3 Ubiquitin Ligases. Annual Review of Biochemistry *78*, 399–434.

Dove, K.K., and Klevit, R.E. (2017). RING-Between-RING E3 Ligases: Emerging Themes amid the Variations. Journal of Molecular Biology *429*, 3363–3375.

Endo, A., Kuroda, M., and Tsujita, Y. (1976). ML-236A, ML-236B, and ML-236C, new inhibitors of cholesterogenesis produced by Penicillium citrinum. The Journal of Antibiotics *XXIX*, 1346–1348.

Esmon, B., Novick, P., and Schekman, R. (1981). Compartmentalized assembly of oligosaccharides on exported glycoproteins in yeast. Cell *25*, 451–460.

Farrell, P., Shi, L., Matuszkiewicz, J., Balakrishna, D., Hoshino, T., Zhang, L., Elliott, S., Fabrey, R., Lee, B., Halkowycz, P., et al. (2013). Biological Characterization of TAK-901, an Investigational, Novel, Multitargeted Aurora B Kinase Inhibitor. Molecular Cancer Therapeutics *12*, 460–470.

Fischer, E.S., Scrima, A., Böhm, K., Matsumoto, S., Lingaraju, G.M., Faty, M., Yasuda, T., Cavadini, S., Wakasugi, M., Hanaoka, F., et al. (2011). The Molecular Basis of CRL4DDB2/CSA Ubiquitin Ligase Architecture, Targeting, and Activation. Cell *147*, 1024–1039.

Fischer, E.S., Böhm, K., Lydeard, J.R., Yang, H., Stadler, M.B., Cavadini, S., Nagel, J., Serluca, F., Acker, V., Lingaraju, G.M., et al. (2014). Structure of the DDB1–CRBN E3 ubiquitin ligase in complex with thalidomide. Nature *512*, 49–53.

Folkes, A.J., Ahmadi, K., Alderton, W.K., Alix, S., Baker, S.J., Box, G., Chuckowree, I.S., Clarke, P.A., Depledge, P., Eccles, S.A., et al. (2008). The Identification of 2-(1H-Indazol-4-yl)-6-(4-methanesulfonyl-piperazin-1-ylmethyl)-4-morpholin-4-yl-thieno[3,2-d]pyrimidine (GDC-0941) as a Potent, Selective, Orally Bioavailable Inhibitor of Class I PI3 Kinase for the Treatment of Cancer. J. Med. Chem. *51*, 5522–5532.

Fortier, J.M., and Kornbluth, J. (2006). NK Lytic-Associated Molecule, Involved in NK Cytotoxic Function, Is an E3 Ligase. J Immunol *176*, 6454–6463.

Freemont, P.S. (1993). The RING Finger. Annals of the New York Academy of Sciences *684*, 174–192.

Fry, D.W., Harvey, P.J., Keller, P.R., Elliott, W.L., Meade, M., Trachet, E., Albassam, M., Zheng, X., Leopold, W.R., Pryer, N.K., et al. (2004). Specific inhibition of cyclin-dependent kinase 4/6 by PD 0332991 and associated antitumor activity in human tumor xenografts. Mol Cancer Ther 12.

Gérard, F.C.A., Yang, R., Romani, B., Poisson, A., Belzile, J.-P., Rougeau, N., and Cohen, É.A. (2014). Defining the Interactions and Role of DCAF1/VPRBP in the DDB1-Cullin4A E3 Ubiquitin Ligase Complex Engaged by HIV-1 Vpr to Induce a G2 Cell Cycle Arrest. PLoS ONE *9*, e89195.

Goldstein, G., Scheid, M., Hammerling, U., Schlesinger, D.H., Niall, H.D., and Boyse, E.A. (1975). Isolation of a polypeptide that has lymphocyte-differentiating properties and is probably represented universally in living cells. PNAS *72*, 11–15.

Guo, Y., Wang, M., Zhang, S., Wu, Y., Zhou, C., Zheng, R., Shao, B., Wang, Y., Xie, L., Liu, W., et al. (2018). Ubiquitin-specific protease USP34 controls osteogenic differentiation and bone formation by regulating BMP2 signaling. EMBO J *37*, e99398.

Hall, J.R., Kow, E., Nevis, K.R., Lu, C.K., Luce, K.S., Zhong, Q., and Cook, J.G. (2007). Cdc6 Stability Is Regulated by the Huwe1 Ubiquitin Ligase after DNA Damage. Molecular Biology of the Cell *18*, 3340–3350.

Han, K., Jeng, E.E., Hess, G.T., Morgens, D.W., Li, A., and Bassik, M.C. (2017). Synergistic drug combinations for cancer identified in a CRISPR screen for pairwise genetic interactions. Nature Biotechnology *35*, 463–474.

Hart, T., Chandrashekhar, M., Aregger, M., Steinhart, Z., Brown, K.R., MacLeod, G., Mis, M., Zimmermann, M., Fradet-Turcotte, A., Sun, S., et al. (2015). High-Resolution CRISPR Screens Reveal Fitness Genes and Genotype-Specific Cancer Liabilities. Cell *163*, 1515–1526.

Hartwell, L.H. (1967). Macromolecule Synthesis in Temperature-sensitive Mutants of Yeast. *93*, 9.

Horlbeck, M.A., Gilbert, L.A., Villalta, J.E., Adamson, B., Pak, R.A., Chen, Y., Fields, A.P., Park, C.Y., Corn, J.E., Kampmann, M., et al. (2016). Compact and highly active next-generation libraries for CRISPR-mediated gene repression and activation. ELife *5*, e19760.

Horlbeck, M.A., Xu, A., Wang, M., Bennett, N.K., Park, C.Y., Bogdanoff, D., Adamson, B., Chow, E.D., Kampmann, M., Peterson, T.R., et al. (2018). Mapping the Genetic Landscape of Human Cells. Cell *174*, 953-967.e22.

Huibregtse, J.M., Scheffner, M., Beaudenon, S., and Howley, P.M. (1995). A family of proteins structurally and functionally related to the E6-AP ubiquitin-protein ligase. PNAS *92*, 2563–2567.

Ito, T., Niwa, J., Hishikawa, N., Ishigaki, S., Doyu, M., and Sobue, G. (2003). Dorfin Localizes to Lewy Bodies and Ubiquitylates Synphilin-1. J. Biol. Chem. *278*, 29106–29114.

Itoh, M., Kim, C.-H., Palardy, G., Oda, T., Jiang, Y.-J., Maust, D., Yeo, S.-Y., Lorick, K., Wright, G.J., Ariza-McNaughton, L., et al. (2003). Mind Bomb Is a Ubiquitin Ligase that Is Essential for Efficient Activation of Notch Signaling by Delta. Developmental Cell *4*, 67–82.

Jinek, M., Chylinski, K., Fonfara, I., Hauer, M., Doudna, J.A., and Charpentier, E. (2012). A Programmable Dual-RNA–Guided DNA Endonuclease in Adaptive Bacterial Immunity. Science *337*, 816–821.

Juszkiewicz, S., and Hegde, R.S. (2017). Initiation of Quality Control during Poly(A) Translation Requires Site-Specific Ribosome Ubiquitination. Mol Cell *65*, 743–750.

Juszkiewicz, S., Chandrasekaran, V., Lin, Z., Kraatz, S., Ramakrishnan, V., and Hegde, R.S. (2018). ZNF598 Is a Quality Control Sensor of Collided Ribosomes. Molecular Cell *72*, 469–481.

Kaneko, C., Hatakeyama, S., Matsumoto, M., Yada, M., Nakayama, K., and Nakayama, K.I. (2003). Characterization of the mouse gene for the U-box-type ubiquitin ligase UFD2a. Biochemical and Biophysical Research Communications *300*, 297–304.

Kasai, S., Arakawa, N., Okubo, A., Shigeeda, W., Yasuhira, S., Masuda, T., Akasaka, T., Shibazaki, M., and Maesawa, C. (2016). NAD(P)H:Quinone Oxidoreductase-1 Expression Sensitizes Malignant Melanoma Cells to the HSP90 Inhibitor 17-AAG. PLOS ONE *11*, e0153181.

Kelsall, I.R., Duda, D.M., Olszewski, J.L., Hofmann, K., Knebel, A., Langevin, F., Wood, N., Wightman, M., Schulman, B.A., and Alpi, A.F. (2013). TRIAD1 and HHARI bind to and are activated by distinct neddylated Cullin-RING ligase complexes. EMBO J *32*, 2848–2860.

Kobirumaki, F., Miyauchi, Y., Fukami, K., and Tanaka, H. (2005). A Novel UbcH10-Binding Protein Facilitates the Ubiquitinylation of Cyclin B In Vitro. Journal of Biochemistry *137*, 133–139.

Koegl, M., Hoppe, T., Schlenker, S., Ulrich, H.D., Mayer, T.U., and Jentsch, S. (1999). A Novel Ubiquitination Factor, E4, Is Involved in Multiubiquitin Chain Assembly. Cell *96*, 635–644.

Koepp, D.M., Schaefer, L.K., Ye, X., Keyomarsi, K., Chu, C., Harper, J.W., and Elledge, S.J. (2001). Phosphorylation-Dependent Ubiquitination of Cyclin E by the SCFFbw7 Ubiquitin Ligase. Science *294*, 173–177.

Komander, D., and Rape, M. (2012). The Ubiquitin Code. Annu. Rev. Biochem. *81*, 203–229.

Komander, D., Clague, M.J., and Urbé, S. (2009). Breaking the chains: structure and function of the deubiquitinases. Nat Rev Mol Cell Biol *10*, 550–563.

Koren, I., Timms, R.T., Kula, T., Xu, Q., Li, M.Z., and Elledge, S.J. (2018). The Eukaryotic Proteome Is Shaped by E3 Ubiquitin Ligases Targeting C-Terminal Degrons. Cell *173*, 1622–1635.

Kudo, N., Matsumori, N., Taoka, H., Fujiwara, D., Schreiner, E.P., Wolff, B., Yoshida, M., and Horinouchi, S. (1999). Leptomycin B inactivates CRM1/exportin 1 by covalent modification at a cysteine residue in the central conserved region. PNAS *96*, 9112–9117.

Lane, D.P., Cheok, C.F., and Lain, S. (2010). p53-based Cancer Therapy. Cold Spring Harb Perspect Biol *2*, a001222.

Li, T., Robert, E.I., van Breugel, P.C., Strubin, M., and Zheng, N. (2010). A promiscuous α-helical motif anchors viral hijackers and substrate receptors to the CUL4–DDB1 ubiquitin ligase machinery. Nat Struct Mol Biol *17*, 105–111.

Li, W., Bengtson, M.H., Ulbrich, A., Matsuda, A., Reddy, V.A., Orth, A., Chanda, S.K., Batalov, S., and Joazeiro, C.A.P. (2008). Genome-Wide and Functional Annotation of Human E3 Ubiquitin Ligases Identifies MULAN, a Mitochondrial E3 that Regulates the Organelle's Dynamics and Signaling. PLoS One *3*.

Li, W., Xu, H., Xiao, T., Cong, L., Love, M.I., Zhang, F., Irizarry, R.A., Liu, J.S., Brown, M., and Liu, X.S. (2014). MAGeCK enables robust identification of essential genes from genome-scale CRISPR/Cas9 knockout screens. Genome Biology *15*, 554.

Lin, C., Xia, J., Gu, Z., Meng, Y., Gao, D., and Wei, S. (2020). Downregulation of USP34 Inhibits the Growth and Migration of Pancreatic Cancer Cells via Inhibiting the PRR11. OncoTargets & Therapy *13*, 1471–1480.

Lin, X., Yang, T., Wang, S., Wang, Z., Yun, Y., Sun, L., Zhou, Y., Xu, X., Akazawa, C., Hong, W., et al. (2014). RILP interacts with HOPS complex via VPS41 subunit to regulate endocytic trafficking. Sci Rep *4*.

Liu, L., Damerell, D.R., Koukouflis, L., Tong, Y., Marsden, B.D., and Schapira, M. (2019). UbiHub: a data hub for the explorers of ubiquitination pathways. Bioinformatics *35*, 2882–2884.

Lorick, K.L., Jensen, J.P., Fang, S., Ong, A.M., Hatakeyama, S., and Weissman, A.M. (1999). RING fingers mediate ubiquitin-conjugating enzyme (E2)-dependent ubiquitination. PNAS *96*, 11364–11369.

Loveless, T.B., Topacio, B.R., Vashisht, A.A., Galaang, S., Ulrich, K.M., Young, B.D., Wohlschlegel, J.A., and Toczyski, D.P. (2015). DNA Damage Regulates Translation through β-TRCP Targeting of CReP. PLoS Genet *11*, e1005292.

Lui, T.T.H., Lacroix, C., Ahmed, S.M., Goldenberg, S.J., Leach, C.A., Daulat, A.M., and Angers, S. (2011). The Ubiquitin-Specific Protease USP34 Regulates Axin Stability and Wnt/ -Catenin Signaling. Molecular and Cellular Biology *31*, 2053–2065.

Lumb, J.H., Li, Q., Popov, L.M., Ding, S., Keith, M.T., Merrill, B.D., Greenberg, H.B., Li, J.B., and Carette, J.E. (2017). DDX6 Represses Aberrant Activation of Interferon-Stimulated Genes. Cell Rep *20*, 819–831.

Mandegar, M.A., Huebsch, N., Frolov, E.B., Shin, E., Truong, A., Olvera, M.P., Chan, A.H., Miyaoka, Y., Holmes, K., Spencer, C.I., et al. (2016). CRISPR Interference Efficiently Induces Specific and Reversible Gene Silencing in Human iPSCs. Cell Stem Cell *18*, 541–553.

Mark, K.G., Simonetta, M., Maiolica, A., Seller, C.A., and Toczyski, D.P. (2014). Ubiquitin Ligase Trapping Identifies an SCFSaf1 Pathway Targeting Unprocessed Vacuolar/Lysosomal Proteins. Molecular Cell *53*, 148–161.

Matsushime, H., Ewen, M.E., Strom, D.K., Kato, J.-Y., Hanks, S.K., Roussel, M.F., and Sherr, C.J. (1992). Identification and properties of an atypical catalytic subunit (p34-PSK-J3/cdk4) for mammalian D type G1 cyclins. Cell *71*, 323–334.

Meacham, G.C., Patterson, C., Zhang, W., Younger, J.M., and Cyr, D.M. (2001). The Hsc70 co-chaperone CHIP targets immature CFTR for proteasomal degradation. Nat Cell Biol *3*, 100–105.

Meyerson, M., and Harlow, E. (1994). Identification of G1 kinase activity for cdk6, a novel cyclin D partner. Mol Cell Biol *14*, 2077–2086.

Meza Gutierrez, F., Simsek, D., Mizrak, A., Deutschbauer, A., Braberg, H., Johnson, J., Xu, J., Shales, M., Nguyen, M., Tamse-Kuehn, R., et al. (2018). Genetic analysis reveals functions of atypical polyubiquitin chains. ELife *7*, e42955.

Misumi, Y., Misumi, Y., Miki, K., Takatsuki, A., Tamura, G., and Ikehara, Y. (1986). Novel blockade by brefeldin A of intracellular transport of secretory proteins in cultured rat hepatocytes. J. Biol. Chem. *261*, 11398–11403.

Moberg, K.H., Bell, D.W., Wahrer, D.C.R., Haber, D.A., and Hariharan, I.K. (2001). Archipelago regulates Cyclin E levels in Drosophila and is mutated in human cancer cell lines. Nature *413*, 311–316.

Oestergaard, V.H., Pentzold, C., Pedersen, R.T., Iosif, S., Alpi, A., Bekker-Jensen, S., Mailand, N., and Lisby, M. (2012). RNF8 and RNF168 but not HERC2 are required for DNA damage-induced ubiquitylation in chicken DT40 cells. DNA Repair *11*, 892–905.

Oh, E., Kim, J.Y., Sung, D., Cho, Y., Lee, N., An, H., Kim, Y.-J., Cho, T.-M., and Seo, J.H. (2017). Inhibition of ubiquitin-specific protease 34 (USP34) induces epithelial-mesenchymal transition and promotes stemness in mammary epithelial cells. Cellular Signalling *36*, 230–239.

Ohi, M.D., Vander Kooi, C.W., Rosenberg, J.A., Chazin, W.J., and Gould, K.L. (2003). Structural insights into the U-box, a domain associated with multi-ubiquitination. Nature Structural & Molecular Biology *10*, 250–255.

Prakash, L. (1981). Characterization of Postreplication Repair in Saccharomyces cerevisiae and Effects of rad6, radl8, rev3 and rad52 Mutations. Molecular Genetics and Genomics *184*, 471–478.

Reid, L.J., Shakya, R., Modi, A.P., Lokshin, M., Cheng, J.-T., Jasin, M., Baer, R., and Ludwig, T. (2008). E3 ligase activity of BRCA1 is not essential for mammalian cell viability or homology-directed repair of double-strand DNA breaks. PNAS *105*, 20876–20881.

Rose, C.M., Isasa, M., Ordureau, A., Prado, M.A., Beausoleil, S.A., Jedrychowski, M.P., Finley, D.J., Harper, J.W., and Gygi, S.P. (2016). Highly Multiplexed Quantitative Mass Spectrometry Analysis of Ubiquitylomes. Cell Systems *3*, 395-403.e4.

Sanjana, N.E., Shalem, O., and Zhang, F. (2014). Improved vectors and genome-wide libraries for CRISPR screening. Nat Methods *11*, 783–784.

Santonico, E., Mattioni, A., Panni, S., Belleudi, F., Mattei, M., Torrisi, M.R., Cesareni, G., and Castagnoli, L. (2015). RNF11 is a GGA protein cargo and acts as a molecular adaptor for GGA3 ubiquitination mediated by Itch. Oncogene *34*, 3377–3390.

Sato, Y., Yoshikawa, A., Yamagata, A., Mimura, H., Yamashita, M., Ookata, K., Nureki, O., Iwai, K., Komada, M., and Fukai, S. (2008). Structural basis for specific cleavage of Lys 63-linked polyubiquitin chains. Nature *455*, 358–362.

Scheffner, M., Nuber, U., and Huibregtse, J.M. (1995). Protein ubiquitination involving an E1–E2–E3 enzyme ubiquitin thioester cascade. Nature *373*, 81–83.

Schulman, B.A., Carrano, A.C., Jeffrey, P.D., Bowen, Z., Kinnucan, E.R.E., Finnin, M.S., Elledge, S.J., Harper, J.W., Pagano, M., and Pavletich, N.P. (2000). Insights into SCF ubiquitin ligases from the structure of the Skp1-Skp2 complex. Nature *408*, 6.

Schumacher, J.M., Golden, A., and Donovan, P.J. (1998). AIR-2: An Aurora/Ipl1-related Protein Kinase Associated with Chromosomes and Midbody Microtubules Is Required for Polar Body Extrusion and Cytokinesis in Caenorhabditis elegans Embryos. The Journal of Cell Biology *143*, 1635–1646.

Segala, G., Bennesch, M.A., Ghahhari, N.M., Pandey, D.P., Echeverria, P.C., Karch, F., Maeda, R.K., and Picard, D. (2019). Vps11 and Vps18 of Vps-C membrane traffic complexes are E3 ubiquitin ligases and fine-tune signalling. Nat Commun *10*, 1833.

Shao, H., Li, X., Moses, M.A., Gilbert, L.A., Kalyanaraman, C., Young, Z.T., Chernova, M., Journey, S.N., Weissman, J.S., Hann, B., et al. (2018). Exploration of Benzothiazole Rhodacyanines as Allosteric Inhibitors of Protein–Protein Interactions with Heat Shock Protein 70 (Hsp70). J. Med. Chem. *61*, 6163–6177.

Shi, J., Wang, E., Milazzo, J.P., Wang, Z., Kinney, J.B., and Vakoc, C.R. (2015). Discovery of cancer drug targets by CRISPR-Cas9 screening of protein domains. Nature Biotechnology *33*, 661–667.

Spence, J., Sadis, S., Haas, A.L., and Finley, D. (1995). A ubiquitin mutant with specific defects in DNA repair and multiubiquitination. Mol. Cell. Biol. *15*, 1265–1273.

Spinette, S., Lengauer, C., Mahoney, J.A., Jallepalli, P.V., Wang, Z., Casciola-Rosen, L., and Rosen, A. (2004). Ufd2, a Novel Autoantigen in Scleroderma, Regulates Sister Chromatid Separation. Cell Cycle *3*, 1612–1618.

Spratt, D.E., Walden, H., and Shaw, G.S. (2014). RBR E3 ubiquitin ligases: new structures, new insights, new questions. Biochemical Journal *458*, 421–437.

Stebbins, C.E., Kaelin Jr., W.G., and Pavletich, N.P. (1999). Structure of the VHL-ElonginC-ElonginB Complex: Implications for VHL Tumor Suppressor Function. Science *284*, 455–461.

Steegmaier, M., Hoffmann, M., Baum, A., Lénárt, P., Petronczki, M., Krššák, M., Gürtler, U., Garin-Chesa, P., Lieb, S., Quant, J., et al. (2007). BI 2536, a Potent and Selective Inhibitor of Polo-like Kinase 1, Inhibits Tumor Growth In Vivo. Current Biology *17*, 316–322.

Stevens, T., Esmon, B., and Schekman, R. (1982). Early stages in the yeast secretory pathway are required for transport of carboxypeptidase Y to the vacuole. Cell *30*, 439–448.

Strohmaier, H., Spruck, C.H., Kaiser, P., Won, K.-A., Sangfelt, O., and Reed, S.I. (2001). Human F-box protein hCdc4 targets cyclin E for proteolysis and is mutated in a breast cancer cell line. Nature *413*, 316–322.

Sudakin, V., Ganoth, D., Dahan, A., Heller, H., Hershko, J., Luca, F.C., Ruderman, J.V., and Hershko, A. (1995). The cyclosome, a large complex containing cyclin-selective ubiquitin ligase activity, targets cyclins for destruction at the end of mitosis. MBoC *6*, 185–197.

Sun, L., Shi, L., Li, W., Yu, W., Liang, J., Zhang, H., Yang, X., Wang, Y., Li, R., Yao, X., et al. (2009). JFK, a Kelch domain-containing F-box protein, links the SCF complex to p53 regulation. PNAS *106*, 10195–10200.

Sundaramoorthy, E., Leonard, M., Mak, R., Liao, J., Fulzele, A., and Bennett, E.J. (2017). ZNF598 and RACK1 Regulate Mammalian Ribosome-Associated Quality Control Function by Mediating Regulatory 40S Ribosomal Ubiquitylation. Molecular Cell *65*, 751-760.e4.

Sy, S.M.H., Jiang, J., O, W.S., Deng, Y., and Huen, M.S.Y. (2013). The ubiquitin specific protease USP34 promotes ubiquitin signaling at DNA double-strand breaks. Nucleic Acids Res *41*, 8572–8580.

Tateishi, S., Sakuraba, Y., Masuyama, S., Inoue, H., and Yamaizumi, M. (2000). Dysfunction of human Rad18 results in defective postreplication repair and hypersensitivity to multiple mutagens. PNAS *97*, 7927–7932.

Thornton, B.R., and Toczyski, D.P. (2006). Precise destruction: an emerging picture of the APC. Genes & Development *20*, 3069–3078.

Thrower, J.S., Hoffman, L., Rechsteiner, M., and Pickart, C.M. (2000). Recognition of the polyubiquitin proteolytic signal. The EMBO Journal *19*, 94–102.

Toledo, C.M., Ding, Y., Hoellerbauer, P., Davis, R.J., Basom, R., Girard, E.J., Lee, E., Corrin, P., Hart, T., Bolouri, H., et al. (2015). Genome-wide CRISPR-Cas9 screens reveal loss of redundancy between PKMYT1 and WEE1 in Glioblastoma stem-like cells. Cell Rep *13*, 2425–2439.

Tong, A.H.Y., Evangelista, M., Parsons, A.B., Xu, H., Bader, G.D., Page, N., Robinson, M., Raghibizadeh, S., Hogue, C.W.V., Bussey, H., et al. (2001). Systematic Genetic Analysis with Ordered Arrays of Yeast Deletion Mutants. Science *294*, 2364–2368.

Tripathy, D., Bardia, A., and Sellers, W.R. (2017). Ribociclib (LEE011): mechanism of action and clinical impact of this selective cyclin-dependent kinase 4/6 inhibitor in various solid tumors. Clin Cancer Res *23*, 3251–3262.

Wang, H.-R., Zhang, Y., Ozdamar, B., Ogunjimi, A.A., Alexandrova, E., Thomsen, G.H., and Wrana, J.L. (2003). Regulation of Cell Polarity and Protrusion Formation by Targeting RhoA for Degradation. Science *302*, 1775–1779.

Wang, T., Birsoy, K., Hughes, N.W., Krupczak, K.M., Post, Y., Wei, J.J., Lander, E.S., and Sabatini, D.M. (2015). Identification and characterization of essential genes in the human genome. Science *350*, 1096–1101.

Wang, T., Yu, H., Hughes, N.W., Liu, B., Kendirli, A., Klein, K., Chen, W.W., Lander, E.S., and Sabatini, D.M. (2017). Gene Essentiality Profiling Reveals Gene Networks and Synthetic Lethal Interactions with Oncogenic Ras. Cell *168*, 890-903.e15.

Welcker, M., and Clurman, B.E. (2008). FBW7 ubiquitin ligase: a tumour suppressor at the crossroads of cell division, growth and differentiation. Nature Reviews Cancer *8*, 83–93.

Welcker, M., Orian, A., Jin, J., Grm, J.E., Harper, J.W., Eisenman, R.N., and Clurman, B.E. (2004). The FBXW7 tumor suppressor regulates glycogen synthase kinase 3 phosphorylation-dependent c-Myc protein degradation. PNAS *101*, 9085–9090.

Xu, G., and Jaffrey, S.R. (2013). Proteomic Identification of Protein Ubiquitination Events. Biotechnol Genet Eng Rev *29*, 73–109.

Yen, H.-C.S., and Elledge, S.J. (2008). Identification of SCF Ubiquitin Ligase Substrates by Global Protein Stability Profiling. Science *322*, 923–929.

Zelcer, N., Hong, C., Boyadjian, R., and Tontonoz, P. (2009). LXR Regulates Cholesterol Uptake through Idol-dependent Ubiquitination of the LDL Receptor. Science *325*, 100–104.

Zheng, N., Schulman, B.A., Song, L., Miller, J.J., Jeffrey, P.D., Wang, P., Chu, C., Koepp, D.M., Elledge, S.J., and Pagano, M. (2002). Structure of the Cul1–Rbx1–Skp1–F boxSkp2 SCF ubiquitin ligase complex. Science *416*, 7.

Zhong, Q., Gao, W., Du, F., and Wang, X. (2005). Mule/ARF-BP1, a BH3-Only E3 Ubiquitin Ligase, Catalyzes the Polyubiquitination of Mcl-1 and Regulates Apoptosis. Cell *121*, 1085–1095.

Zhu, H., Kavsak, P., Abdollah, S., Wrana, J.L., and Thomsen, G.H. (1999). A SMAD ubiquitin ligase targets the BMP pathway and affects embryonic pattern formation. Nature *400*, 687–693.

**Publishing Agreement**

It is the policy of the University to encourage open access and broad distribution of all theses, dissertations, and manuscripts. The Graduate Division will facilitate the distribution of UCSF theses, dissertations, and manuscripts to the UCSF Library for open access and distribution. UCSF will make such theses, dissertations, and manuscripts accessible to the public and will take reasonable steps to preserve these works in perpetuity.

I hereby grant the non-exclusive, perpetual right to The Regents of the University of California to reproduce, publicly display, distribute, preserve, and publish copies of my thesis, dissertation, or manuscript in any form or media, now existing or later derived, including access online for teaching, research, and public service purposes.

DocuSigned by:
Frances Hundley
ACF6F343BF92477...
Author Signature

11/27/2020
Date